Manuscript prepared for Geosci. Model Dev.
with version 2014/07/29 7.12 Copernicus papers of the LaTeX class copernicus.cls.
Date: 3 May 2017

OMEN-SED 1.0: A new, numerically efficient sediment module for the coupling to Earth System Models

Dominik Hülse[1], Sandra Arndt[1, 2], Stuart Daines[3], Andy Ridgwell[1, 4], and Pierre Regnier[2]

[1]School of Geographical Sciences, University of Bristol, Clifton, Bristol BS8 1SS, UK
[2]Department of Earth and Environmental Sciences, Université Libre de Bruxelles, Brussels, Belgium
[3]Earth System Science, University of Exeter, North Park Road, Exeter EX4 4QE, UK
[4]Department of Earth Sciences, University of California, Riverside, CA 92521, USA

Correspondence to: Dominik Hülse (Dominik.Huelse@bristol.ac.uk)

Abstract. Here we describe the first version of the Organic Matter ENabled SEDiment model (OMEN-SED 1.0).

Contents

1 Introduction

DH: How to include comments.

Role of marine sediments for climate and global biogeochemical cycles:

Marine surface sediments are key components in the Earth system. They host the largest carbon reservoir within the surficial Earth system, provide the only long term sink for atmospheric CO_2, recycle nutrients and represent the most important geochemical archive used for deciphering past changes in biogeochemical cycles and climate. Physical and chemical processes in sediments (i.e. diagenetic processes) depend on the water column and vice versa: Diagenesis is mainly donor controlled, as it is fuelled by the external supply of solid material (e.g. organic matter, calcium carbonate, opal) from the water column and is affected by overlying bottom water concentrations of solutes. At the same time, diagenesis in the sediments transforms the deposited material and returns some of the resulting products (e.g. nutrients, DIC) to the water column. This so-called benthic-pelagic coupling is essential for understanding global biogeochemical cycles and climate (e.g. Archer and Maier-Reimer, 1994; Soetaert et al., 2000; Archer et al., 2000; Mackenzie, 2005).

Biological primary production of organic matter (OM, CH_2O in equation R1) and the reverse process of degradation can be written in a greatly simplified reaction as:

$$CO_2 + H_2O \rightleftharpoons CH_2O + O_2. \tag{R1}$$

On geological timescales production of OM is generally greater than degradation which results in some organic matter being buried in marine sediments and oxygen accumulating in the atmosphere. Thus burial of OM leads to net oxygen input to, and CO_2 removal from the atmosphere (Berner, 2004). On shorter timescales, the upper few meters of the sediments (i.e. early diagenesis) are specifically important as it is decided here if a substance is recycled to the water column or buried for a longer period of time in the deeper sediments (Hensen et al., 2006). Most biogeochemical cycles and reactions in this part of marine sediments can be related either directly or indirectly to the degradation of organic matter (e.g Boudreau and Ruddick, 1991; Arndt et al., 2013). Organic matter degradation releases metabolic CO_2 to the pore water, causing it to have a lower pH and provoking the dissolution of $CaCO_3$ (Emerson and Bender, 1981). Oxygen and nitrate for instance, the most powerful electron acceptors, are consumed in the course of the degradation of organic matter, resulting in the release of ammonium and phosphate to the pore water. As such, changes in the degradation rate of OM can profoundly affect the oxygen and nutrient inventory of the ocean and thus primary productivity (Van Cappellen and Ingall, 1994; Lenton and Watson, 2000).

TODO include info on shelf-nutrient hypothesis: (From Palastanga et al. 2013) During glacial periods, P burial on shelves was likely reduced because of sea level fall, whereas the erosive transfer of particulate material containing reactive P and degradable carbon from shelves to the open ocean was likely enhanced (Ruttenberg,1993). As a consequence, the inventory of P in the open ocean, primary productivity and CO2 drawdown may have increased, whereas ocean oxygen may have declined. This potential impact on productivity and CO2 was first brought forward by Broecker

(1982) in the so-called shelf-nutrient hypothesis. Nutrient recycling from the sediments has been invoked by modelling and data studies to explain the occurance of extreme events in Earth history, for instance Oceanic Anoxic Events (OAEs) (e.g. Mort et al., 2007; Tsandev and Slomp, 2009). OAEs represent severe disturbances of the global carbon, oxygen and nutrient cycles of the ocean and are usually characterized by widespread bottom water anoxia and photic zone euxinia (Jenkyns, 2010). One way to explain the genesis and persistence of OAEs is increased oxygen demand due to enhanced primary productivity (PP). Increased nutrient inputs to fuel PP may have come from marine sediments as the burial efficiency of phosphorus declines when bottom waters become anoxic (Ingall and Jahnke, 1994; Van Cappellen and Ingall, 1994). The recovery from OAE like conditions is thought to involve the permanent removal of excess CO_2 from the atmosphere and ocean by burying carbon in the form of organic matter in marine sediments (e.g. Arthur et al., 1988; Jarvis et al., 2011), which is consistent with the geological record of widespread black shale formation (Stein et al., 1986). However, the overall amount, exact timing and the rate of organic matter burial remain a topic of an ongoing debate.

Diagenetic Models:

Therefore, globally quantifying the burial and degradation of organic matter in marine sediments and related biogeochemical dynamics is important for understanding climate and the cycling of many chemical elements on various timescales. Such studies and quantifications are possible through the application of idealised mathematical representations of diagenesis, or so-called diagenetic models (e.g. Berner, 1980; Boudreau, 1997). The number of research questions that can be addressed with diagenetic models is infinite and a plethora of different approaches have been developed, mainly following two distinct directions (Arndt et al., 2013). First, state-of-the art vertically resolved diagenetic models simulating the entire suite of the essential coupled redox and equilibrium reactions within marine sediments that control carbon burial and benthic recycling fluxes (e.g. BRNS, Aguilera et al., 2005; CANDI, Boudreau, 1996; MEDIA, Meysman et al., 2003). These "complete", non-steady-state models, thus explicitly include oxic OM mineralisation, denitrification, oxidation by manganese and iron (hydr)oxides, sulphate reduction and methanogenesis as well as the reoxidation of reduced byproducts formed in the mineralization of OM (i.e. NH_4, Mn^{2+}, Fe^{2+}, H_2S, CH_4). Furthermore, they incorporate various mineral dissolution and precipitation reactions, as well as adsorption and desorption processes for example of NH_4 and PO_4. Modelled, depth dependent, transport processes usually comprise advection, diffusion, bioturbation and bio-irrigation. Diagenetic models generally use a so-called multi-G approach, thus dividing the bulk organic carbon pool into a number of compound classes that are characterised by different degradabilities k_i, which are generally dependent on the type and concentration of the specific terminal electron acceptor (TEA) used. Due to the large number of interrelated processes and depth dependent parameters diagenetic models need to be solved numerically, thus resulting in a very high computational demand.

elaborate on the capabilities of existing numerical models and clearly highlight that omensed captures most of these features (the best examples are the possibility to account for the full suite of secondary redox reactions and also the simulation of pH).

Combining such a complex diagenetic model with an ocean biogeochemical model results in the most realistic benthic-pelagic coupling. However, the global applicability of this set-up is limited by the high computation cost of simulating all biogeochemical reactions in the sediments. The second group of models is less sophisticated and comprehensive than the "complete", non-steady-state diagenetic models and is used for the coupling to global Earth System Models (e.g. DCESS, Shaffer et al., 2008; MEDUSA, Munhoven, 2007 or the model of Heinze et al. (1999)). In particular, these analytic models consider fewer biogeochemical reactions and assume that the sedimentary organic matter pool is composed of just a single or two discrete compound classes (1G or 2G approach respectively).

How are sediments resolved in Earth System models:

Even though there is potential to use more appropriate global sediment representations, in most current Earth System models (ESMs) sediment-water exchange of OM and chemical elements is either neglected or treated in a very simplistic way (Soetaert et al., 2000; Hülse et al., 2017). Most Earth system Models of Intermediate Complexity (EMICs) and also some of the higher resolution global carbon cycle models represent the sediment-water interface either as a reflective or a conservative/semi-reflective boundary (Hülse et al., 2017). Thus, all particulate material deposited on the seafloor is either instantaneously consumed (reflective boundary), or a fixed fraction is buried in the sediments (conservative/semi-reflective boundary). Both highly simplified approaches furthermore completely neglect the exchange of solute species through the sediment-water interface and, therefore, cannot resolve the complex benthic-pelagic coupling. However, due to their computational efficiency, both representations are often used in global biogeochemical models (e.g. Najjar et al., 2007; Ridgwell et al., 2007; Goosse et al., 2010). A superior approach is the vertically integrated dynamic model, which represents the whole sediment column as a single box (Hülse et al., 2017). Here, OM deposited on the seafloor is added to the sediment box where it gets degraded and dissolved species diffuse through the sediment-water interface in accordance with these transformations. This approach thus ignores the vertical extent of the sediments and the temporary storage of dissolved species (Soetaert et al., 2000). Yet, it is computationally efficient and also allows differentiating between various fractions of organic matter. Most EMICs incorporate a vertically integrated dynamic model for particulate inorganic carbon only (i.e. mainly $CaCO_3$) and just a few consider oxic-only sediment degradation of organic matter (Hülse et al., 2017). The most complex description of marine sediments in Earth System models are vertically resolved diagenetic models, solving the one-dimensional, fully coupled reaction-transport equation for multiple solid and dissolved species (e.g. Berner, 1980; Boudreau, 1997). These models account for important transport processes (e.g. bioturbation, molecular diffusion and bioirrigation), resolve the coupled biogeochemical dynamics

of dissolved species and usually at least a part of the resulting characteristic redox-zonation of marine sediments (Soetaert et al., 2000). Examples of global carbon cycle models employing a vertically resolved diagenetic model are PISCES (Gehlen et al., 2006) and CLIMBER 3α (Ilyina et al., 2013), both using a version of Heinze et al. (1999), however, just utilizing a 1G approach with a constant degradation rate constant. None of the EMICs reviewed by Hülse et al. (2017) use such a sediment representation. elaborate on the existing vertically resolved models and clearly highlight what are the key novel features of omensed

Problem with that:

Obviously, such simplifications can neither account for the observed vast structural complexity in natural organic matter and its resulting different degradation rates nor for the rapid decrease in OM degradability in the uppermost centimeters of the sediments (Arndt et al., 2013). At least a 3G approach is necessary to accurately represent organic matter dynamics in this part of the sediments where most OM is degraded (e.g. Soetaert et al., 1996b). Furthermore, the spatial variability in benthic OM degradation kinetics is unknown at the global scale and reported rate constants can vary by almost 10 orders of magnitude (Arndt et al., 2013). Thus, a major challenge for diagenetic models is defining appropriate OM degradation rate constants which is either achieved through profile fitting for a specific site or, for global applications, the rate constants follow empirical relations with a related, readily available sediment characteristic such as water depth (Middelburg et al., 1997), sedimentation rate (Toth and Lerman, 1977; Tromp et al., 1995) or OM flux (Boudreau, 1997). However, these relationships are mostly based on simple fitting exercises to limited data sets and show at the most a very weak trend and no statistically significant relationship (Arndt et al., 2013). This creates considerable uncertainties when diagenetic models are coupled to global biogeochemical ocean models especially when applying the model for different geological timescales. Other model parameters implicitly accounting for processes not explicitly described are sedimentation and bioturbation rate and are generally related to water depth following Middelburg et al. (1997).

Solution presented here:

Say OMEN-SED is a compromise between numerical diagentic models and existing vertically resolved models currently used for the coupling to ESMs. highlight the key novel features of omensed and that it captures most of the features of numerical diagenetic models, however, mostly in an depth independent way

Here, we present the OrganicMatter ENabled SEDiment model (OMEN-SED 1.0), a new, one-dimensional, numerically efficient reactive transport model (RTM) that describes OM cycling as well as the associated dynamics of the most important TEAs (i.e. O_2, NO_3, SO_4, CH_4), related reduced substances (NH_4 H_2S), macronutrients (PO_4) and associated pore water quantities (ALK, DIC). OMEN-SED's computational efficiency allows its coupling to Earth System Models of different complexities and therefore the investigation of coupled global biogeochemical dynamics over geological timescales. Here, the model is presented as a 2G-approach, however, a third, nondegrad-

able OM pool can be added and furthermore OMEN-SED can easily be extended to a Multi-G approach.

2 Model Description

The following section provides a detailed description of the new model. Table 1 summarizes the biogeochemical reaction network and a glossary of parameters along with their respective units is provided in Tables 9 and 10.

2.1 General Model Approach

The calculation of benthic return/uptake and burial fluxes is based on the vertically resolved conservation equation for solid and dissolved species in porous media (e.g. Berner, 1980; Boudreau, 1997):

$$\frac{\partial \xi C_i}{\partial t} = -\frac{\partial F}{\partial z} + \xi \sum_j R_i^j \tag{1}$$

where C_i is the concentration of the biogeochemical species i, ξ equals the porosity ϕ for solute species and $(1-\phi)$ for solid species, hence represents the partitioning of species i into the solute and dissolved phase. The term z is the sediment depth, t denotes the time, F summarises the transport fluxes and $\sum_j R_i^j$ represents the sum of production/consumption rates j that affect species i. The reaction network accounts for the most important primary and secondary redox reactions, equilibrium reactions, mineral dissolution and precipitation, as well as adsorption and desorption processes that affect the explicitly resolved chemical species.

State-of-the-art reaction-transport models generally solve the ordinary differential equation (ODE, Eq. 1) numerically and thus allow to account for transient dynamics, depth-varying parameters or a high degree of coupling between different chemical species (e.g. Soetaert et al., 1996b; Aguilera et al., 2005). Yet, numerical models are computational expensive, thus rendering their application in an Earth System Model framework prohibitive. An analytical solution of equation (1) provides an alternative and computational more efficient approach which enjoyed great popularity in the early days of diagenetic modelling and computer technology. However, early analytical models were often very problem-specific and only considered one or two coupled species (e.g. Berner, 1964). (e.g. Lehrman, Berner) ?? which other pub? Over the next decades, a number of more complex analytical models describing the coupled dynamics of OM degradation, TEAs and rediced substances in sediments were developed (e.g. Billen, 1982; Goloway and Bender, 1982; Jahnke et al., 1982), before the boost in computing power enabled the development of fully-coupled, multi-species, numerical models (e.g. Van Cappellen and Wang, 1995; Soetaert et al., 1996b).

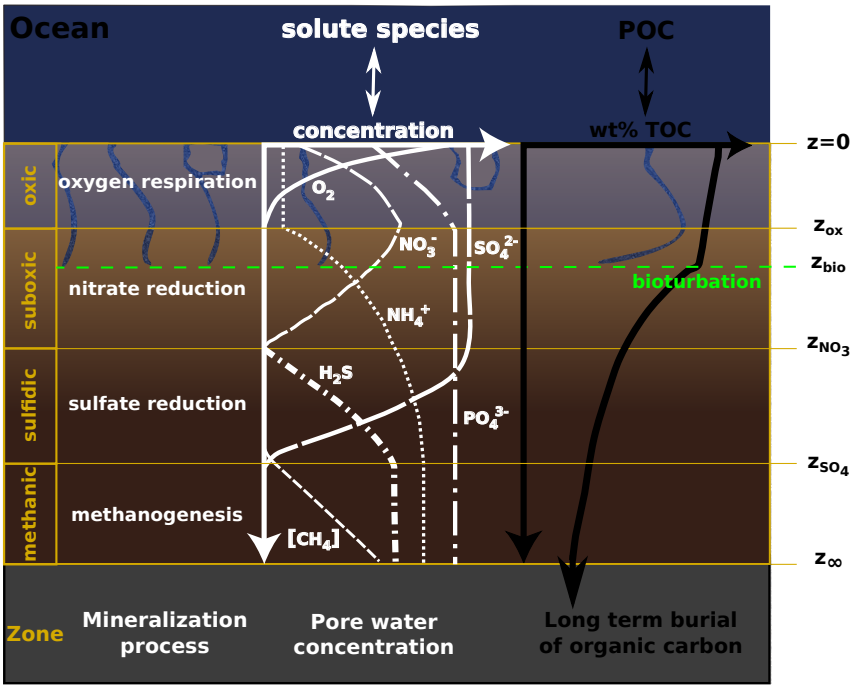

Figure 1. Schematic of the different modelled species and layers in OMEN-SED. Here showing the case $z_{\mathrm{ox}} < z_{\mathrm{bio}} < z_{\mathrm{NO_3}} < z_{\mathrm{SO_4}}$.

Finding an analytical solution to Eq. (1), especially when complex reaction networks are to be considered, is not straightforward and generally requires the assumption of steady state. In addition, the complexity of the reaction network can be reduced by dividing the sediment into distinct zones and accounting for the most pertinent biogeochemical processes within each zone, thus increasing the likelihood of finding an analytical solution to Eq. (1) (see Eq. (30) in section 2.5.1 for the general steady-state solution).

Therefore, OMEN-SED assumes that benthic dynamics can be represented by a series of steady-states. Because the Earth system model relevant variability in boundary conditions and fluxes is generally longer than the characteristic timescales of the reaction-transport processes, the sediment can be described by a series of pseudo steady-states. In addition, it divides the sediment into a bioturbated and a non-bioturbated zone defined by the constant bioturbation depth z_{bio} (see Fig. 1). Furthermore, it accounts for the dynamic redox zonation of marine sediments by dividing the sediment into: 2) an oxic zone delineated by the oxygen penetration depth z_{ox}, 3) a denitrification zone situated between z_{ox} and the nitrate penetration depth $z_{\mathrm{NO_3}}$, 4) a sulfate reduction zone situated between $z_{\mathrm{NO_3}}$ and the sulfate penetration depth $z_{\mathrm{SO_4}}$ and 5) a methanogenic zone situated below $z_{\mathrm{SO_4}}$ (Fig. 1). All penetration depths are dynamically calculated by the model. Each zone is characterised

by a set of diagenetic equations that encapsulate the most pertinent reaction and transport processes in this zone (see section 2.2 and 2.3 for more details).

OMEN calculates and feeds back to the Earth System model the fraction of POC preserved in the sediments and the sediment-water interface fluxes of the dissolved species C_i (in mol cm^{-2} year^{-1}):

$$\mathrm{Flux\_SWI(C_i)} = \phi \left(D_i \frac{\partial C_i(z)}{\partial z}\bigg|_0 - w\left[C_i(0) - C_i(z_\infty)\right] \right) \tag{2}$$

where w is the deposition rate, D_i is the diffusion coefficient and $C_i(0),\ C_i(z_\infty)$ the concentration of species i at the SWI and at the lower sediment boundary.

2.2 Transport

The model accounts for both the advective, as well as the diffusive transport of dissolved and solid species, assuming that sediment compaction is negligible (i.e. $\frac{\partial \phi}{\partial z} = 0$). The molecular diffusion of dissolved species is described via a species-specific apparent diffusion coefficient, $D_{\mathrm{mol},i}$. In addition, the activity of infaunal organisms in the bioturbated zone of the sediment ($z < z_{\mathrm{bio}}$) that causes random displacements of sediments and porewaters is simulated using a diffusive term (e.g. Boudreau,1986), with a constant bioturbation coefficient D_{bio} in the bioturbated zone. The pumping activity by burrow-dwelling animals and the resulting ventilation of tubes, the so-called bioirrigation, is encapsulated in a factor, f_{ir} that enhances the molecular diffusion coefficient (hence, $D_{i,0} = D_{\mathrm{mol},i} \cdot f_{ir}$, Soetaert et al., 1996a). The flux divergence can thus be formulated as:

$$\frac{\partial F}{\partial z} = -\frac{\partial}{\partial z}\left(-\xi D_i \frac{\partial C_i}{\partial z} + \xi w C_i \right) \tag{3}$$

where D_i is the diffusion coefficient of species i ($D_i = D_{i,0} + D_{\mathrm{bio}} = D_{\mathrm{mol},i} \cdot f_{ir} + D_{\mathrm{bio}}$ for dissolved species and $D_i = D_{\mathrm{bio}}$ for solid species) and w is the deposition rate. The bioturbation coefficient D_{bio} is set to zero below z_{bio}.

2.3 Reaction Network

Earth System models generally track the biogeochemical dynamics of organic and inorganic carbon, essential nutrients (nitrogen, phosphorus) and oxygen with the aim of investigating the evolution of the ocean's redox structure and carbonate system and its feedbacks on global climate. This general aim thus defines a minimum set of state variables and reaction processes that need to be resolved for an efficient representation of the benthic-pelagic coupling in Earth system models. A suitable sediment model must provide a robust quantification of organic (and inorganic) carbon burial fluxes, as well as the benthic return fluxes of growth-limiting nutrients, equilibrium invariant and reduced species, and oxygen uptake fluxes. As a consequence, the reaction network must account for the most important primary and secondary redox reactions, equilibrium reactions, mineral precipitation/dissolution and adsorption/desorption, resulting in a complex set of coupled reaction-transport

Table 1. Reactions and biogeochemical tracers implemented in the Reaction Network of OMEN-SED. The primary and secondary redox reactions are listed in the sequence they occur with increasing sediment depth.

	Description
Primary redox reactions	Degradation of organic matter via aerobic respiration, denitrification, sulfate reduction, methanogenesis (implicit)
Secondary redox reactions	Oxidation of ammonium and sulfide by oxygen, anaerobic oxidation of methane by sulfate
Adsorption/Desorption	Ad-/Desorption of P on/from $\mathrm{Fe(OH)_3}$, $\mathrm{NH_4}$ adsorption, $\mathrm{PO_4}$ adsorption
Mineral precipitation	Formation of authigenic P
Biogeochemical tracers	Organic matter, oxygen, nitrate, ammonium, sulfate, sulfide (hydrogen sulfide), phosphate, Fe-bound P, DIC, ALK

equations. The following subsections provide a short discussion of the reaction processes included in the model and give an overview of the vertically resolved conservation equations and boundary conditions for solid and dissolved species in each layer. Table 1 provides a summary of the reactions and biogeochemical tracers considered in the reaction network. Table 15 summarises their reaction stoichiometry and Table **??** provides an overview of their description in the model.

2.3.1 Organic matter or Particulate Organic Carbon (POC)

In marine sediments, organic matter (OM) is degraded by heterotrophic activity coupled to the sequential utilisation of terminal electron acceptors, typically in the order of $\mathrm{O_2}$, $\mathrm{NO_3^-}$, $\mathrm{Mn(VI)}$, $\mathrm{Fe(III)}$ and $\mathrm{SO_4^{2-}}$ followed by methanogenesis and/or fermentation. Here, organic matter degradation is described via a multi-G model approach (Arndt et al., 2013, and references therein), assuming that the bulk OM consists of a number of discrete compound classes C_i characterised by specific degradation rate constants k_i. Such a multi-G approach allows for selective preservation of compound classes according to their reactivity, k_i and, thus, accounts for the change in organic matter reactivity during burial. Each compound class is degraded according to first-order kinetics. The conservation equation for organic matter dynamics is thus given by:

$$\frac{\partial C_i}{\partial t} = 0 = D_{C_i}\frac{\partial^2 C_i}{\partial z^2} - w\frac{\partial C_i}{\partial z} - k_i \cdot C_i \tag{4}$$

The analytical solution of Eq. (4) (see section 2.5 for details) requires the definition of a set of boundary conditions (Table 2). The model assumes a known concentration/flux at the sediment-water interface and continuity across the bottom of the bioturbated zone, z_{bio}.

Table 2. Boundary conditions for organic matter. For the boundaries we define: $z^-_{\mathrm{bio}} := \lim_{h\to 0}(z_{\mathrm{bio}} - h)$ and $z^+_{\mathrm{bio}} := \lim_{h\to 0}(z_{\mathrm{bio}} + h)$.

Boundary	**Condition**	
$z = 0$	known concentration	1) $C_i(0) = C_{i0}$
$z = z_{\mathrm{bio}}$	continuity	2) $C_i(z^-_{\mathrm{bio}})$=$C_i(z^+_{\mathrm{bio}})$
		3) $-D_{\mathrm{bio}} \cdot \frac{\partial C_i}{\partial z}\vert_{z^-_{\mathrm{bio}}} = 0$

2.3.2 Oxygen

In marine sediments, oxygen is consumed via aerobic degradation of organic matter and a number of secondary redox reactions. In the oxic layer ($z < z_{ox}$), the model explicitly accounts for the aerobic degradation of OM, which consumes oxygen with a fixed O_2 : C ratio (O_2C, Tab. 10) and produces ammonium, which is partially nitrified to nitrate (γ_{NH_4}). In addition, the oxygen consumption due to oxidation of reduced species (NH_4, H_2S) produced in the suboxic and anoxic layers of the sediment is implicitly taken into account through the flux boundary condition at the dynamic oxygen penetration depth z_{ox}. This simplification can be justified as it has been shown that these secondary redox reactions mainly occur at the oxic/suboxic interface (Soetaert et al., 1996b). The factor $\frac{1-\phi}{\phi}$ accounts for the volume conversion from the solid to the dissolved phase. Oxygen dynamics are thus described by:

$$\frac{\partial \mathrm{O_2}}{\partial t} = 0 = D_{\mathrm{O_2}} \frac{\partial^2 \mathrm{O_2}}{\partial z^2} - w \frac{\partial \mathrm{O_2}}{\partial z} - \frac{1-\phi}{\phi} \sum_i k_i \cdot [\mathrm{O_2C} + 2\gamma_{\mathrm{NH_4}} \mathrm{NC_i}] \cdot C_i(z) \tag{5}$$

The analytical solution of Eq. (5) requires the definition of boundary conditions (Table 3). OMEN-SED assumes a known bottom water concentration and the complete consumption of oxygen at the oxygen penetration depth (or zero flux if $z_{\mathrm{ox}} = z_\infty$). Equal oxygen concentration and diffusive flux above (z^-_{bio}) and below (z^+_{bio}) the bioturbation boundary is considered. In addition, the model accounts for reduced species produced by anaerobic mineralization diffusing into the oxic layer from below, assuming that respective fractions ($\gamma_{\mathrm{NH_4}}$ and $\gamma_{\mathrm{H_2S}}$) are re-oxidised at the oxic/suboxic interface.

2.3.3 Nitrate and Ammonium

To model nitrate and ammonium dynamics the sediment is partitioned into two geochemical layers (oxic and suboxic), where different equations describe the biogeochemical processes. Above the oxygen penetration depth organic matter mineralization produces ammonium, which is partly nitrified to nitrate (the fraction $\gamma_{\mathrm{NH_4}}$). In the suboxic zone ($z > z_{\mathrm{ox}}$), oxygen concentration is zero and nitrate serves as the electron acceptor to respire organic matter, thus nitrate is consumed by denitrification and ammonium is produced. Below the nitrate penetration depth $z_{\mathrm{NO_3}}$, ammonium is still produced via OM mineralization. The model assumes that adsorption of ammonium to sediment

Table 3. Boundary conditions for oxygen. For the boundaries we define: $z^-_{\mathrm{bio}} := \lim_{h\to 0}(z_{\mathrm{bio}} - h)$ and $z^+_{\mathrm{bio}} := \lim_{h\to 0}(z_{\mathrm{bio}} + h)$.

Boundary	**Condition**	
$z = 0$	known concentration	1) $\mathrm{O_2}(0) = O_{20}$
$z = z_{\mathrm{bio}}$	continuity	2) $\mathrm{O_2}(z^-_{\mathrm{bio}})$=$\mathrm{O_2}(z^+_{\mathrm{bio}})$
		3) $-(D_{\mathrm{O_2},0} + D_{\mathrm{bio}}) \cdot \frac{\partial \mathrm{O_2}}{\partial z}\big|_{z^-_{\mathrm{bio}}} = -D_{\mathrm{O_2},0} \cdot \frac{\partial \mathrm{O_2}}{\partial z}\big|_{z^+_{\mathrm{bio}}}$
$z = z_{\mathrm{ox}}$	$\mathrm{O_2}$ consumption	4) **IF** $(\mathrm{O_2}(z_\infty) > 0)$
	($z_{\mathrm{ox}} = z_\infty$)	$\frac{\partial \mathrm{O_2}}{\partial z}|_{z_{\mathrm{ox}}} = 0$
		ELSE
	($z_{\mathrm{ox}} < z_\infty$)	$\mathrm{O_2}(z_{\mathrm{ox}}) = 0$ and $-D_{\mathrm{O_2}} \cdot \frac{\partial \mathrm{O_2}}{\partial z}|_{z_{\mathrm{ox}}} = F_{red}(z_{\mathrm{ox}})$
	with flux from below	$F_{red}(z_{\mathrm{ox}}) = \frac{1-\phi}{\phi} \cdot \int_{z_{\mathrm{ox}}}^{\infty} \sum_i (2\gamma_{\mathrm{NH_4}}\mathrm{NC_i} + 2\gamma_{\mathrm{H_2S}}\mathrm{SO_4C})\, k_i C_i \, dz$

particles is fast compared with the characteristic transport time scales. Thus, a constant equilibrium adsorption coefficient $K_{\mathrm{NH_4}}$ is used to parameterize the loss of dissolved $\mathrm{NH_4}$ to adsorped $\mathrm{NH_4}$ (Wang and Van Cappellen, 1996). Therefore the diagenetic equations for nitrate and ammonium are given by:

1. Layer ($z \le z_{\mathrm{ox}}$)

$$\frac{\partial NO_3^I}{\partial t} = 0 = D_{NO_3}\frac{\partial^2 NO_3^I}{\partial z^2} - w\frac{\partial NO_3^I}{\partial z} + \gamma_{\mathrm{NH_4}}\frac{1-\phi}{\phi} \cdot \sum_i \mathrm{NC_i} \cdot k_i \cdot C_i(z) \tag{6}$$

$$\frac{\partial \mathrm{NH_4}^I}{\partial t} = 0 = \frac{D_{\mathrm{NH_4}}}{1+K_{\mathrm{NH_4}}}\frac{\partial^2 \mathrm{NH_4}^I}{\partial z^2} - w\frac{\partial \mathrm{NH_4}^I}{\partial z} + \frac{1-\gamma_{\mathrm{NH_4}}}{1+K_{\mathrm{NH_4}}} \cdot \frac{1-\phi}{\phi} \cdot \sum_i \mathrm{NC_i} \cdot k_i \cdot C_i(z) \tag{7}$$

2. Layer ($z_{\mathrm{ox}} < z \le z_{\mathrm{NO_3}}$)

$$\frac{\partial NO_3^{II}}{\partial t} = 0 = D_{NO_3}\frac{\partial^2 NO_3^{II}}{\partial z^2} - w\frac{\partial NO_3^{II}}{\partial z} - \frac{1-\phi}{\phi} NO_3C \cdot \sum_i k_i \cdot C_i(z) \tag{8}$$

$$\frac{\partial \mathrm{NH_4}^{II}}{\partial t} = 0 = \frac{D_{\mathrm{NH_4}}}{1+K_{\mathrm{NH_4}}}\frac{\partial^2 \mathrm{NH_4}^{II}}{\partial z^2} - w\frac{\partial \mathrm{NH_4}^{II}}{\partial z} \tag{9}$$

3. Layer ($z_{\mathrm{NO_3}} < z \le z_\infty$)

$$\frac{\partial \mathrm{NH_4}^{III}}{\partial t} = 0 = \frac{D_{\mathrm{NH_4}}}{1+K_{\mathrm{NH_4}}}\frac{\partial^2 \mathrm{NH_4}^{III}}{\partial z^2} - w\frac{\partial \mathrm{NH_4}^{III}}{\partial z} + \frac{1}{1+K_{\mathrm{NH_4}}} \cdot \frac{1-\phi}{\phi} \cdot \sum_i \mathrm{NC_i} \cdot k_i \cdot C_i(z) \tag{10}$$

The boundary conditions to solve Equations 6 - 10 are summarized in Table 4. The model assumes known bottom water concentrations for both species, the complete consumption of nitrate at the nitrate penetration depth (or zero flux if $z_{\mathrm{NO_3}} = z_\infty$) and no change in ammonium flux at z_∞. It considers equal concentrations and diffusive fluxes at z_{bio} and z_{ox}. In addition, the re-oxidation of upward-diffusing reduced ammonium is considered in the oxic-suboxic boundary condition for nitrate and ammonium.

Table 4. Boundary conditions for nitrate and ammonium. For the boundaries we define: $z_{\_}^{-} := \lim_{h\to 0}(z_{\_} - h)$ and $z_{\_}^{+} := \lim_{h\to 0}(z_{\_} + h)$.

Boundary	**Condition**	
$z = 0$	known concentration	1) $NO_3(0) = NO_{30}$
$z = z_{\mathrm{bio}}$	continuity	2) $NO_3(z_{\mathrm{bio}}^{-})$=$NO_3(z_{\mathrm{bio}}^{+})$
		3) $-(D_{NO_3,0} + D_{\mathrm{bio}}) \cdot \frac{\partial NO_3}{\partial z}\vert_{z_{\mathrm{bio}}^{-}} = -D_{NO_3,0} \cdot \frac{\partial NO_3}{\partial z}\vert_{z_{\mathrm{bio}}^{+}}$
$z = z_{\mathrm{ox}}$	continuity	4) $NO_3(z_{\mathrm{ox}}^{-})$=$NO_3(z_{\mathrm{ox}}^{+})$
		5) $-D_{NO_3} \cdot \frac{\partial NO_3}{\partial z}\vert_{z_{\mathrm{ox}}^{-}} + \gamma_{\mathrm{NH_4}} \cdot F_{\mathrm{NH_4}}(z_{\mathrm{ox}}) = -D_{NO_3} \cdot \frac{\partial NO_3}{\partial z}\vert_{z_{\mathrm{ox}}^{+}}$
	where:	$F_{\mathrm{NH_4}}(z_{\mathrm{ox}}) = \frac{1}{1+K_{\mathrm{NH_4}}} \cdot \frac{1-\phi}{\phi} \cdot \int_{z_{\mathrm{NO_3}}}^{\infty} \sum_i k_i \cdot \mathrm{NC_i} \cdot C_i \, dz$
$z = z_{\mathrm{NO_3}}$	$\mathrm{NO_3}$ consumption	6) **IF** $(\mathrm{NO_3}(z_\infty) > 0)$
	$(z_{\mathrm{NO_3}} = z_\infty)$	$\frac{\partial NO_3}{\partial z}\vert_{z_{\mathrm{NO_3}}} = 0$
		ELSE
	$(z_{\mathrm{NO_3}} < z_\infty)$	$NO_3(z_{\mathrm{NO_3}}) = 0$
$z = 0$	known concentration	1) $\mathrm{NH_4}(0) = \mathrm{NH_{40}}$
$z = z_{\mathrm{bio}}$	continuity	2) $\mathrm{NH_4}(z_{\mathrm{bio}}^{-})$=$\mathrm{NH_4}(z_{\mathrm{bio}}^{+})$
		3) $-\frac{D_{\mathrm{NH_4},0}+D_{\mathrm{bio}}}{1+K_{\mathrm{NH_4}}} \cdot \frac{\partial \mathrm{NH_4}}{\partial z}\vert_{z_{\mathrm{bio}}^{-}} = -\frac{D_{\mathrm{NH_4},0}}{1+K_{\mathrm{NH_4}}} \cdot \frac{\partial \mathrm{NH_4}}{\partial z}\vert_{z_{\mathrm{bio}}^{+}}$
$z = z_{\mathrm{ox}}$	continuity	4) $\mathrm{NH_4}(z_{\mathrm{ox}}^{-})$=$\mathrm{NH_4}(z_{\mathrm{ox}}^{+})$
		5) $-\frac{D_{\mathrm{NH_4}}}{1+K_{\mathrm{NH_4}}} \cdot \frac{\partial \mathrm{NH_4}}{\partial z}\vert_{z_{\mathrm{ox}}^{-}} - \gamma_{\mathrm{NH_4}} \cdot F_{\mathrm{NH_4}}(z_{\mathrm{ox}}) = -\frac{D_{\mathrm{NH_4}}}{1+K_{\mathrm{NH_4}}} \cdot \frac{\partial \mathrm{NH_4}}{\partial z}\vert_{z_{\mathrm{ox}}^{+}}$
	where:	$F_{\mathrm{NH_4}}(z_{\mathrm{ox}}) = \frac{1}{1+K_{\mathrm{NH_4}}} \cdot \frac{1-\phi}{\phi} \cdot \int_{z_{\mathrm{NO_3}}}^{\infty} \sum_i k_i \cdot \mathrm{NC_i} \cdot C_i \, dz$
$z = z_{\mathrm{NO_3}}$	continuity	6) $\mathrm{NH_4}(z_{\mathrm{NO_3}}^{-})$=$\mathrm{NH_4}(z_{\mathrm{NO_3}}^{+})$
	flux	7) $-\frac{D_{\mathrm{NH_4}}}{1+K_{\mathrm{NH_4}}} \cdot \frac{\partial \mathrm{NH_4}}{\partial z}\vert_{z_{\mathrm{NO_3}}^{-}} = -\frac{D_{\mathrm{NH_4}}}{1+K_{\mathrm{NH_4}}} \cdot \frac{\partial \mathrm{NH_4}}{\partial z}\vert_{z_{\mathrm{NO_3}}^{+}}$
$z = z_\infty$	zero $\mathrm{NH_4}$ flux	8) $\frac{\partial \mathrm{NH_4}}{\partial z}\vert_{z_\infty} = 0$

2.3.4 Sulfate and Sulfide

When nitrate is depleted, sulfate reduction is the pathway to mineralize organic matter, thus consuming sulfate ($\mathrm{SO_4}$) and producing hydrogen sulfide ($\mathrm{H_2S}$) until the sulfate penetration depth ($z_{\mathrm{SO_4}}$). Sulfate and sulfide dynamics are thus described by:

1. Layer ($z \le z_{\mathrm{NO_3}}$)

$$\frac{\partial \mathrm{SO_4}^{I}}{\partial t} = 0 = D_{\mathrm{SO_4}} \frac{\partial^2 \mathrm{SO_4}^{I}}{\partial z^2} - w \frac{\partial \mathrm{SO_4}^{I}}{\partial z} \tag{11}$$

$$\frac{\partial \mathrm{H_2S}^{I}}{\partial t} = 0 = D_{\mathrm{H_2S}} \frac{\partial^2 \mathrm{H_2S}^{I}}{\partial z^2} - w \frac{\partial \mathrm{H_2S}^{I}}{\partial z} \tag{12}$$

2. Layer ($z_{\mathrm{NO_3}} < z \le z_{\mathrm{SO_4}}$)

$$\frac{\partial \mathrm{SO_4}^{II}}{\partial t} = 0 = D_{\mathrm{SO_4}} \frac{\partial^2 \mathrm{SO_4}^{II}}{\partial z^2} - w \frac{\partial \mathrm{SO_4}^{II}}{\partial z} - \frac{1-\phi}{\phi} \cdot \sum_i \mathrm{SO_4C} \cdot k_i \cdot C_i(z) \tag{13}$$

$$\frac{\partial \mathrm{H_2S}^{II}}{\partial t} = 0 = D_{\mathrm{H_2S}} \frac{\partial^2 \mathrm{H_2S}^{II}}{\partial z^2} - w \frac{\partial \mathrm{H_2S}^{II}}{\partial z} + \frac{1-\phi}{\phi} \cdot \sum_i \mathrm{SO_4C} \cdot k_i \cdot C_i(z) \tag{14}$$

3. Layer ($z_{SO_4} < z \leq z_\infty$)

$$\frac{\partial H_2S^{III}}{\partial t} = 0 = D_{H_2S}\frac{\partial^2 H_2S^{III}}{\partial z^2} - w\frac{\partial H_2S^{III}}{\partial z} \quad (15)$$

To solve equations 11 - 15 the model assumes known concentrations at the sediment-water interface and continuity across the bioturbation depth and the nitrate penetration depth (see Table 5). The re-oxidation of reduced H_2S to SO_4 is considered in the oxic-suboxic boundary condition for both species, here including the methanic zone, as H_2S is also produced during anaerobic oxidation of methane (AOM). Furthermore, sulfate is used at z_{SO_4} to oxidize methane from below and thus producing H_2S. In case $z_{SO_4} < z_\infty$, sulfate concentration is zero at z_{SO_4} and its diffusive flux must equal the amount of methane produced below; or, in case $z_{SO_4} = z_\infty$, a zero flux condition for sulfate is considered. At the lower boundary z_∞ zero flux of H_2S is considered. correct??

2.3.5 Phosphate

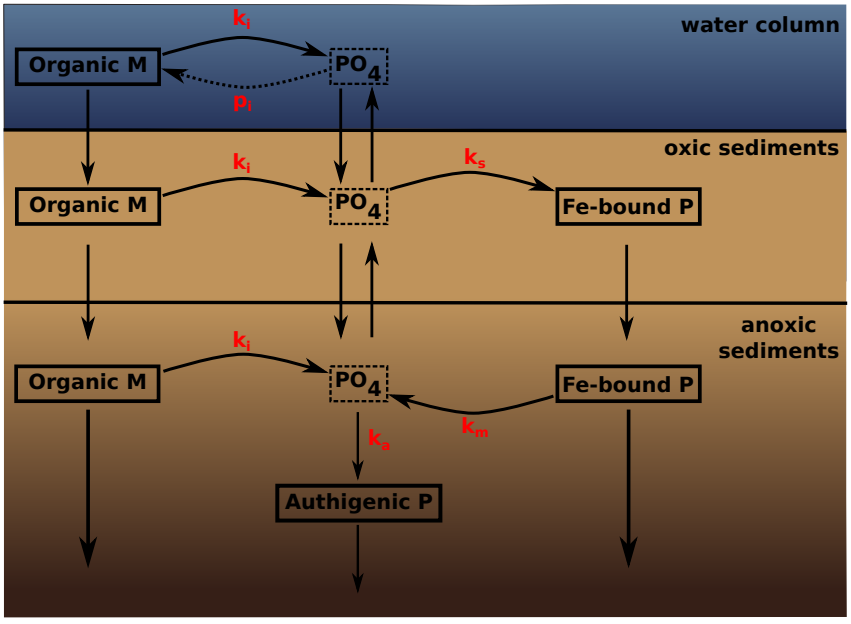

Figure 2. A schematic of the sedimentary P cycle in OMEN-SED. Red numbers represent kinetic rate constants for phosphorus dynamics (compare Table 10; p_i represents uptake rate of PO_4 via primary production in shallow environments). Adapted from Slomp et al. (1996).

To model phosphorus (P) dynamics in the sediments OMEN-SED takes into account the change with depth of phosphate (PO_4) and iron-bound P, thereby mainly following the description of Slomp et al. (1996) and Gypens et al. (2008). Throughout the sediment column organic matter is mineralized resulting in a release of phosphate to the pore water. In the oxic part of the sediment, this PO_4

Table 5. Boundary conditions for sulfate and sulfide. For the boundaries we define: $z_{\_}^{-} := \lim_{h\to 0}(z_{\_} - h)$ and $z_{\_}^{+} := \lim_{h\to 0}(z_{\_} + h)$.

Boundary	**Condition**		
$z = 0$	known concentration	1)	$SO_4(0)$=SO_{40}
$z = z_{\mathrm{bio}}$	continuity	2)	$SO_4(z_{\mathrm{bio}}^{-})$=$SO_4(z_{\mathrm{bio}}^{+})$
	flux	3)	$-(D_{SO_4,0} + D_{\mathrm{bio}}) \cdot \frac{\partial SO_4}{\partial z}\vert_{z_{\mathrm{bio}}^{-}} = -D_{SO_4,0} \cdot \frac{\partial SO_4}{\partial z}\vert_{z_{\mathrm{bio}}^{+}}$
$z = z_{\mathrm{ox}}$	continuity	4)	$SO_4(z_{\mathrm{ox}}^{-})$=$SO_4(z_{\mathrm{ox}}^{+})$
	flux	5)	$-D_{SO_4} \cdot \frac{\partial SO_4}{\partial z}\vert_{z_{\mathrm{ox}}^{-}} + \gamma_{H_2S} \cdot F_{H_2S}(z_{\mathrm{ox}}) = -D_{SO_4} \cdot \frac{\partial SO_4}{\partial z}\vert_{z_{\mathrm{ox}}^{+}}$
	where:		$F_{H_2S}(z_{\mathrm{ox}}) = \frac{1-\phi}{\phi} \cdot \left(\int_{z_{NO_3}}^{SO_4} \sum_i SO_4C \cdot k_i \cdot C_i \, dz + \gamma_{CH_4} \cdot \int_{z_{SO_4}}^{\infty} \sum_i MC \cdot k_i \cdot C_i \, dz \right)$
$z = z_{NO_3}$	continuity	6)	$SO_4(z_{NO_3}^{-})$=$SO_4(z_{NO_3}^{+})$
	flux	7)	$-D_{SO_4} \cdot \frac{\partial SO_4}{\partial z}\vert_{z_{NO_3}^{-}} = -D_{SO_4} \cdot \frac{\partial SO_4}{\partial z}\vert_{z_{NO_3}^{+}}$
$z = z_{SO_4}$	SO_4 consumption	8)	**IF** $(SO_4(z_\infty) > 0)$
	$(z_{SO_4} = z_\infty)$		$\frac{\partial SO_4}{\partial z}\vert_{z_{SO_4}} = 0$
			ELSE
	$(z_{SO_4} < z_\infty)$		$SO_4(z_{SO_4}) = 0$ and $-D_{SO_4} \cdot \frac{\partial SO_4}{\partial z}\vert_{z_{SO_4}} = \gamma_{CH_4} \cdot F_{CH_4}(z_{SO_4})$
	with flux from below:		$F_{CH_4}(z_{SO_4}) = \frac{1-\phi}{\phi} \cdot \int_{z_{SO_4}}^{\infty} \sum_i MC \cdot k_i \cdot C_i \, dz$
$z = 0$	known concentration	1)	$H_2S(0) = H_2S_0$
$z = z_{\mathrm{bio}}$	continuity	2)	$H_2S(z_{\mathrm{bio}}^{-})$=$H_2S(z_{\mathrm{bio}}^{+})$
	flux	3)	$-(D_{H_2S,0} + D_{\mathrm{bio}}) \cdot \frac{\partial H_2S}{\partial z}\vert_{z_{\mathrm{bio}}^{-}} = -D_{H_2S,0} \cdot \frac{\partial H_2S}{\partial z}\vert_{z_{\mathrm{bio}}^{+}}$
$z = z_{\mathrm{ox}}$	continuity	4)	$H_2S(z_{\mathrm{ox}}^{-})$=$H_2S(z_{\mathrm{ox}}^{+})$
	flux	5)	$-D_{H_2S} \cdot \frac{\partial H_2S}{\partial z}\vert_{z_{\mathrm{ox}}^{-}} - \gamma_{H_2S} F_{H_2S}(z_{\mathrm{ox}}) = -D_{H_2S} \cdot \frac{\partial H_2S}{\partial z}\vert_{z_{\mathrm{ox}}^{+}}$
	where:		$F_{H_2S}(z_{\mathrm{ox}}) = \frac{1-\phi}{\phi} \cdot \left(\int_{z_{NO_3}}^{SO_4} \sum_i SO_4C \cdot k_i \cdot C_i \, dz + \gamma_{CH_4} \cdot \int_{z_{SO_4}}^{\infty} \sum_i MC \cdot k_i \cdot C_i \, dz \right)$
$z = z_{NO_3}$	continuity	6)	$H_2S(z_{NO_3}^{-})$=$H_2S(z_{NO_3}^{+})$
	flux	7)	$-D_{H_2S} \cdot \frac{\partial H_2S}{\partial z}\vert_{z_{NO_3}^{-}} = -D_{H_2S} \cdot \frac{\partial H_2S}{\partial z}\vert_{z_{NO_3}^{+}}$
$z = z_{SO_4}$	continuity	8)	$H_2S(z_{SO_4}^{-})$=$H_2S(z_{SO_4}^{+})$
	flux (with AOM)	9)	$-D_{H_2S} \cdot \frac{\partial H_2S}{\partial z}\vert_{z_{SO_4}^{-}} + \gamma_{CH_4} \cdot F_{CH_4}(z_{SO_4}) = -D_{H_2S} \cdot \frac{\partial H_2S}{\partial z}\vert_{z_{SO_4}^{+}}$
	where:		$F_{CH_4}(z_{SO_4}) = \frac{1-\phi}{\phi} \cdot \int_{z_{SO_4}}^{\infty} \sum_i MC \cdot k_i \cdot C_i \, dz$
$z = z_\infty$	zero H_2S flux	10)	$\frac{\partial H_2S}{\partial z}\vert_{z_\infty} = 0$

DH: @Sandra: BC 5) Include $\int_{z_{SO_4}}^{\infty}$ here?

DH: @Sandra: think yes, because at 8) CH_4 from $\int_{z_{SO_4}}^{\infty}$ is oxidised to H_2S; at 5) this H_2S to SO_4

either diffuses upward to the water column or is adsorped to Fe oxides forming Fe-bound P (or M) (Slomp et al., 1998). In the suboxic/anoxic zone, PO_4 is not only produced via organic matter degradation but is also released from the Fe-bound P pool due to the reduction of Fe oxides. Furthermore, phosphate concentrations can become high enough in this layer for authigenic mineral formation to occur (Van Cappellen and Berner, 1988). This phosphorus bound in authigenic minerals represents a permanent sink for reactive phosphorus (Slomp et al., 1996). See Figure 2 for a schematic overview of the sedimentary P cycle. As for ammonium, the adsorption of P to the sediment matrix is treated as an equilibrium processes, parameterized with dimensionless adsorption coefficients for the oxic and anoxic zone ($K^I_{\mathrm{PO_4}}$, $K^{II}_{\mathrm{PO_4}}$ Slomp et al., 1998). Therefore the diagenetic equations for phosphate are written as:

1. Layer ($z \leq z_{\mathrm{ox}}$)

$$\frac{\partial {\mathrm{PO_4}}^I}{\partial t} = \frac{D_{\mathrm{PO_4}}}{1+K^I_{\mathrm{PO_4}}}\frac{\partial^2 {\mathrm{PO_4}}^I}{\partial z^2} - w\frac{\partial {\mathrm{PO_4}}^I}{\partial z} + \frac{1-\phi}{\phi}\frac{1}{1+K^I_{\mathrm{PO_4}}}\sum_i(\mathrm{PC}_i \cdot k_i \cdot C_i(z)) - \frac{k_s}{1+K^I_{\mathrm{PO_4}}}({\mathrm{PO_4}}^I - {\mathrm{PO_4}}^s) \tag{16}$$

$$\frac{\partial M^I}{\partial t} = D_M\frac{\partial^2 M^I}{\partial z^2} - w\frac{\partial M^I}{\partial z} + \frac{\phi}{1-\phi}k_s({\mathrm{PO_4}}^I - {\mathrm{PO_4}}^s) \tag{17}$$

2. Layer ($z_{\mathrm{ox}} < z$)

$$\frac{\partial M^{II}}{\partial t} = D_M\frac{\partial^2 M^{II}}{\partial z^2} - w\frac{\partial M^{II}}{\partial z} - k_m(M^{II} - M^\infty) \tag{18}$$

$$\frac{\partial {\mathrm{PO_4}}^{II}}{\partial t} = \frac{D_{\mathrm{PO_4}}}{1+K^{II}_{\mathrm{PO_4}}}\frac{\partial^2 {\mathrm{PO_4}}^{II}}{\partial z^2} - w\frac{\partial {\mathrm{PO_4}}^{II}}{\partial z} + \frac{1-\phi}{\phi}\frac{1}{1+K^{II}_{\mathrm{PO_4}}}\sum_i(\mathrm{PC}_i \cdot k_i \cdot C_i(z)) - \frac{k_a}{1+K^{II}_{\mathrm{PO_4}}}({\mathrm{PO_4}}^{II} - {\mathrm{PO_4}}^a) + \frac{(1-\phi)}{\phi}\frac{k_m}{1+K^{II}_{\mathrm{PO_4}}}(M^{II} - M^\infty) \tag{19}$$

$$\tag{20}$$

The boundary conditions to solve Equations 16 - 19 are summarized in Table 6. The model assumes known bottom water concentrations and equal concentrations and diffusive fluxes at z_{bio} and z_{ox} for both species. Additionally it considers no change in phosphate flux and an assymptotic Fe-bound P concentration at z_∞.

2.3.6 Dissolved Inorganic Carbon (DIC)

Organic matter degradation produces dissolved inorganic carbon (DIC) with a stoichiometric DIC:C ratio of 1:2 in the methanic zone and 1:1 in the rest of the sediment column. DIC dynamics in OMEN-SED are thus described by equations 21 and 21 and boundary conditions as summarized in Table 7. The model assumes a known DIC concentration at the sediment-water interface, a zero flux condition

Table 6. Boundary conditions for phosphate and Fe-bound P (M). For the boundaries we define: $z_{\_}^{-} := \lim_{h\to 0}(z_{\_} - h)$ and $z_{\_}^{+} := \lim_{h\to 0}(z_{\_} + h)$.

Boundary	**Condition**	
$z = 0$	known concentration	1) $\mathrm{PO_4}(0)$=$\mathrm{PO_{40}}$
$z = z_{\mathrm{bio}}$	continuity	2) $\mathrm{PO_4}(z_{\mathrm{bio}}^{-})$=$\mathrm{PO_4}(z_{\mathrm{bio}}^{+})$
	flux	3) $(D_{\mathrm{PO_4},0} + D_{\mathrm{bio}}) \cdot \frac{\partial \mathrm{PO_4}}{\partial z}\vert_{z_{\mathrm{bio}}^{-}} = D_{\mathrm{PO_4},0} \cdot \frac{\partial \mathrm{PO_4}}{\partial z}\vert_{z_{\mathrm{bio}}^{+}}$
$z = z_{\mathrm{ox}}$	continuity	4) $\mathrm{PO_4}(z_{\mathrm{ox}}^{-})$=$\mathrm{PO_4}(z_{\mathrm{ox}}^{+})$
	flux	5) $-\frac{D_{\mathrm{PO_4}}}{1+K_{\mathrm{PO_4}}^{I}} \cdot \frac{\partial \mathrm{PO_4}}{\partial z}\vert_{z_{\mathrm{ox}}^{-}} = -\frac{D_{\mathrm{PO_4}}}{1+K_{\mathrm{PO_4}}^{II}} \cdot \frac{\partial \mathrm{PO_4}}{\partial z}\vert_{z_{\mathrm{ox}}^{+}}$
$z = z_{\infty}$	flux	10) $\frac{\partial \mathrm{PO_4}}{\partial z}\vert_{z_{\infty}} = 0$
$z = 0$	known concentration	1) $M(0) = M_0$
$z = z_{\mathrm{bio}}$	continuity	2) $M(z_{\mathrm{bio}}^{-})$=$M(z_{\mathrm{bio}}^{+})$
	flux	3) $\frac{\partial M}{\partial z}\vert_{z_{\mathrm{bio}}^{-}} = \frac{\partial M}{\partial z}\vert_{z_{\mathrm{bio}}^{+}}$
$z = z_{\mathrm{ox}}$	continuity	4) $M(z_{\mathrm{ox}}^{-})$=$M(z_{\mathrm{ox}}^{+})$
	flux	5) $\frac{\partial M}{\partial z}\vert_{z_{\mathrm{ox}}^{-}} = \frac{\partial M}{\partial z}\vert_{z_{\mathrm{ox}}^{+}}$
$z = z_{\infty}$	assymptotic concentration	10) $M(z_{\infty}) = M_{\infty}$

at the lower boundary z_{∞} and continuity across the bioturbation and sulfate penetration depth. In addition, the anaerobic oxidation of methane at $z_{\mathrm{SO_4}}$ produces DIC (with 1:1 stoichiometry) which is accounted for through the flux boundary condition at $z_{\mathrm{SO_4}}$ (Table 7 eq. 5)

1. Layer ($z \leq z_{\mathrm{SO_4}}$)

$$\frac{\partial DIC^{I}}{\partial t} = 0 = D_{DIC}\frac{\partial^2 DIC^{I}}{\partial z^2} - w\frac{\partial DIC^{I}}{\partial z} + \frac{1-\phi}{\phi} \cdot \sum_i \mathrm{DICC^{I}} \cdot k_i \cdot C_i(z) \tag{21}$$

2. Layer ($z_{\mathrm{SO_4}} < z \leq z_{\infty}$)

$$\frac{\partial DIC^{II}}{\partial t} = 0 = D_{DIC}\frac{\partial^2 DIC^{II}}{\partial z^2} - w\frac{\partial DIC^{II}}{\partial z} + \frac{1-\phi}{\phi} \cdot \sum_i \mathrm{DICC^{II}} \cdot k_i \cdot C_i(z) \tag{22}$$

2.3.7 Alkalinity

Organic matter degradation and secondary redox reactions exert a complex influence on alkalinity with opposite effects depending on the TEA involved (Wolf-Gladrow et al., 2007). To model alkalinity in OMEN-SED the sediment column is partitioned into four geochemical layers, where different equations describe the biogeochemical processes using variable stoichiometric coefficients (compare Tables 10 and 15). Above z_{ox}, the combined effects of $\mathrm{NH_4}$ and P release due to aerobic OM mineralization increases alkalinity according to $\mathrm{ALK^{OX}}$ whereas nitrification decreases alkalinity with stoichiometry $\mathrm{ALK^{NIT}}$. In the remaining three zones anaerobic OM mineralization increases

Table 7. Boundary conditions for DIC. For the boundaries we define: $z_{\_}^{-} := \lim_{h\to 0}(z_{\_} - h)$ and $z_{\_}^{+} := \lim_{h\to 0}(z_{\_} + h)$.

Boundary	**Condition**	
$z = 0$	known concentration	1) $\mathrm{DIC}(0) = \mathrm{DIC}_0$
$z = z_{\mathrm{bio}}$	continuity	2) $\mathrm{DIC}(z_{\mathrm{bio}}^{-})$=$\mathrm{DIC}(z_{\mathrm{bio}}^{+})$
	flux	3) $-(D_{\mathrm{DIC},0} + D_{\mathrm{bio}}) \cdot \frac{\partial \mathrm{DIC}}{\partial z}\big\vert_{z_{\mathrm{bio}}^{-}} = -D_{\mathrm{DIC},0} \cdot \frac{\partial \mathrm{DIC}}{\partial z}\big\vert_{z_{\mathrm{bio}}^{+}}$
$z = z_{\mathrm{SO_4}}$	continuity	4) $\mathrm{DIC}(z_{\mathrm{SO_4}}^{-})$=$\mathrm{DIC}(z_{\mathrm{SO_4}}^{+})$
	flux (with AOM)	5) $-D_{\mathrm{DIC}} \cdot \frac{\partial \mathrm{DIC}}{\partial z}\big\vert_{z_{\mathrm{SO_4}}^{-}} + \gamma_{\mathrm{CH_4}} \cdot F_{\mathrm{CH_4}}(z_{\mathrm{SO_4}}) = -D_{\mathrm{DIC}} \cdot \frac{\partial \mathrm{DIC}}{\partial z}\big\vert_{z_{\mathrm{SO_4}}^{+}}$
	where:	$F_{\mathrm{CH_4}}(z_{\mathrm{SO_4}}) = \frac{1-\phi}{\phi} \cdot \int_{z_{\mathrm{SO_4}}}^{\infty} \sum_i \mathrm{MC} \cdot k_i \cdot C_i \, dz$
$z = z_{\infty}$	zero DIC flux	6) $\frac{\partial \mathrm{DIC}}{\partial z}\big\vert_{z_{\infty}} = 0$

alkalinity with variable stoichiometric coefficients (i.e. $\mathrm{ALK}^{\mathrm{DEN}}$, $\mathrm{ALK}^{\mathrm{SUL}}$, $\mathrm{ALK}^{\mathrm{MET}}$). Thus, the diagenetic equations for alkalinity are written as:

1. Layer ($z \le z_{\mathrm{ox}}$)

$$\frac{\partial \mathrm{ALK}^{I}}{\partial t} = 0 = D_{\mathrm{ALK}} \frac{\partial^2 \mathrm{ALK}^{I}}{\partial z^2} - w \frac{\partial \mathrm{ALK}^{I}}{\partial z} + \frac{1-\phi}{\phi} \cdot \sum_i \left(\mathrm{ALK}^{\mathrm{NIT}} \cdot \frac{\gamma_{\mathrm{NH_4}}}{1 + K_{\mathrm{NH_4}}} \mathrm{NC_i} + \mathrm{ALK}^{\mathrm{OX}} \right) \cdot k_i \cdot C_i(z) \tag{23}$$

2. Layer ($z_{\mathrm{ox}} < z \le z_{\mathrm{NO_3}}$)

$$\frac{\partial \mathrm{ALK}^{II}}{\partial t} = 0 = D_{\mathrm{ALK}} \frac{\partial^2 \mathrm{ALK}^{II}}{\partial z^2} - w \frac{\partial \mathrm{ALK}^{II}}{\partial z} + \frac{1-\phi}{\phi} \cdot \sum_i \mathrm{ALK}^{\mathrm{DEN}} \cdot k_i \cdot C_i(z) \tag{24}$$

3. Layer ($z_{\mathrm{NO_3}} < z \le z_{\mathrm{SO_4}}$)

$$\frac{\partial \mathrm{ALK}^{III}}{\partial t} = 0 = D_{\mathrm{ALK}} \frac{\partial^2 \mathrm{ALK}^{III}}{\partial z^2} - w \frac{\partial \mathrm{ALK}^{III}}{\partial z} + \frac{1-\phi}{\phi} \cdot \sum_i \mathrm{ALK}^{\mathrm{SUL}} \cdot k_i \cdot C_i(z) \tag{25}$$

4. Layer ($z_{\mathrm{SO_4}} < z \le z_{\infty}$)

$$\frac{\partial \mathrm{ALK}^{IV}}{\partial t} = 0 = D_{\mathrm{ALK}} \frac{\partial^2 \mathrm{ALK}^{IV}}{\partial z^2} - w \frac{\partial \mathrm{ALK}^{IV}}{\partial z} + \frac{1-\phi}{\phi} \cdot \sum_i \mathrm{ALK}^{\mathrm{MET}} \cdot k_i \cdot C_i(z) \tag{26}$$

To solve equations 23 - 26 the model assumes a known concentration at the sediment-water interface and continuity across the bioturbation depth and the penetration depths of O_2, NO_3 and SO_4 (see Table 8). The decrease of alkalinity due to oxidation of reduced species produced in the suboxic and anoxic layers (with stoichiometry $\mathrm{ALK}^{\mathrm{NIT}}$ and $\mathrm{ALK}^{\mathrm{H_2S}}$) is implicitly taken into account through the flux boundary condition at z_{ox} (Table 8 Eq. 5). Furthermore, the oxidation of methane by sulphate reduction increases alkalinity with stoichiometry $\mathrm{ALK}^{\mathrm{AOM}}$ which is accounted for through the flux boundary condition at $z_{\mathrm{SO_4}}$ (Table 8 eq. 9). At the lower boundary z_{∞} a zero flux condition is applied.

Table 8. Boundary conditions for alkalinity. For the boundaries we define: $z_{\_}^{-} := \lim_{h\to 0}(z_{\_} - h)$ and $z_{\_}^{+} := \lim_{h\to 0}(z_{\_} + h)$.

Boundary	**Condition**		
$z = 0$	known concentration	1)	$\mathrm{ALK}(0) = \mathrm{ALK}_0$
$z = z_{\mathrm{bio}}$	continuity	2)	$\mathrm{ALK}(z_{\mathrm{bio}}^{-})$=$\mathrm{ALK}(z_{\mathrm{bio}}^{+})$
	flux	3)	$-(D_{\mathrm{ALK},0} + D_{\mathrm{bio}}) \cdot \frac{\partial \mathrm{ALK}}{\partial z}\vert_{z_{\mathrm{bio}}^{-}} = -D_{\mathrm{ALK},0} \cdot \frac{\partial \mathrm{ALK}}{\partial z}\vert_{z_{\mathrm{bio}}^{+}}$
$z = z_{\mathrm{ox}}$	continuity	4)	$\mathrm{ALK}(z_{\mathrm{ox}}^{-})$=$\mathrm{ALK}(z_{\mathrm{ox}}^{+})$
	flux	5)	$-D_{\mathrm{ALK}} \cdot \frac{\partial \mathrm{ALK}}{\partial z}\vert_{z_{\mathrm{ox}}^{-}} + F_{\mathrm{ALK}}(z_{\mathrm{ox}}) = -D_{\mathrm{ALK}} \cdot \frac{\partial \mathrm{ALK}}{\partial z}\vert_{z_{\mathrm{ox}}^{+}}$
	where:		$F_{\mathrm{ALK}}(z_{\mathrm{ox}}) = \frac{1-\phi}{\phi} \cdot \left(\mathrm{ALK}^{\mathrm{H_2S}} \cdot \gamma_{\mathrm{H_2S}} \int_{z_{\mathrm{NO_3}}}^{\mathrm{SO_4}} \sum_i \mathrm{SO_4C} \cdot k_i \cdot C_i \, dz\right)$ $+ \frac{1-\phi}{\phi} \cdot \left(\mathrm{ALK}^{\mathrm{NIT}} \frac{\gamma_{\mathrm{NH_4}}}{1+k_{\mathrm{NH_4}}} \int_{z_{\mathrm{NO_3}}}^{\infty} \sum_i \mathrm{NC_i} \cdot k_i \cdot C_i \, dz\right)$
$z = z_{\mathrm{NO_3}}$	continuity	6)	$\mathrm{ALK}(z_{\mathrm{NO_3}}^{-})$=$\mathrm{ALK}(z_{\mathrm{NO_3}}^{+})$
	flux	7)	$-D_{\mathrm{ALK}} \cdot \frac{\partial \mathrm{ALK}}{\partial z}\vert_{z_{\mathrm{NO_3}}^{-}} = -D_{\mathrm{ALK}} \cdot \frac{\partial \mathrm{ALK}}{\partial z}\vert_{z_{\mathrm{NO_3}}^{+}}$
$z = z_{\mathrm{SO_4}}$	continuity	8)	$\mathrm{ALK}(z_{\mathrm{SO_4}}^{-})$=$\mathrm{ALK}(z_{\mathrm{SO_4}}^{+})$
	flux (with AOM)	9)	$-D_{\mathrm{ALK}} \cdot \frac{\partial \mathrm{ALK}}{\partial z}\vert_{z_{\mathrm{SO_4}}^{-}} + F_{\mathrm{ALK}}(z_{\mathrm{SO_4}}) = -D_{\mathrm{ALK}} \cdot \frac{\partial \mathrm{ALK}}{\partial z}\vert_{z_{\mathrm{SO_4}}^{+}}$
	where:		$F_{\mathrm{ALK}}(z_{\mathrm{SO_4}}) = \frac{1-\phi}{\phi} \cdot \left(\mathrm{ALK}^{\mathrm{AOM}} \gamma_{\mathrm{CH_4}} \cdot \int_{z_{\mathrm{SO_4}}}^{\infty} \sum_i k_i \cdot C_i \, dz\right)$
$z = z_{\infty}$	zero ALK flux	10)	$\frac{\partial \mathrm{ALK}}{\partial z}\vert_{z_{\infty}} = 0$

2.4 Model Parameters

This section describes the parameters used in OMEN-SED to describe sediment transport and biogeochemical reactions related to the burial and mineralization of organic matter under a wide range of environmental conditions. Table 9 states the parameters for sediment characteristics and table 10 summarizes the stoichiometric factors and secondary reaction parameters used in the model.

2.4.1 Transport Parameters

Advection is the bulk flow of sediments and can be directly related to the accumulation of new material on the seafloor (i.e. sedimentation, Burdige, 2006). This results in a downward flux of older sediment material and porewater in relation to the sediment-water interface. When coupled to an ocean model, its sedimentation flux can be readily used in OMEN-SED 1.0. The stand-alone version of OMEN-SED 1.0 uses the empirical global relationship between sediment accumulation rate (cm yr^{-1}) and seafloor depth (m) of Middelburg et al. (1997):

$$w = 3.3 \cdot 10^{-0.87478367 - 0.00043512 \cdot \mathrm{depth}}, \tag{27}$$

As discussed before (Sec. 2.2), the diffusion coefficient of species i is calculated as $D_i = D_{i,0} + D_{\mathrm{bio}} = D_{\mathrm{mol},i} \cdot f_{ir} + D_{\mathrm{bio}}$ for dissolved species and $D_i = D_{\mathrm{bio}}$ for solid species. The bioturbation coefficient D_{bio} (cm^2 yr$^-$1) is constant in the bioturbated zone and also follows the empirical rela-

tionship by Middelburg et al. (1997):

$$D_{\mathrm{bio}} = 5.2 \cdot 10^{0.76241122 - 0.00039724 \cdot \mathrm{depth}} \tag{28}$$

Studies showed that bioturbational effects on a global scale are largely restricted to the upper 10 cm of the sediments and are only marginally related to seafloor depth (e.g. Boudreau, 1998; Teal et al., 2010). Therefore, OMEN-SED imposes a globally invariant bioturbation depth z_{bio} of 10 cm. In case the bottom water oxygen concentration is below 5 nanomole cm^{-3} infaunnal activity ceases and $z_{\mathrm{bio}} = 0.01$ cm.

Bioirrigation can enhance the molecular diffusion coefficient $D_{i,0} = D_{\mathrm{mol},i} \cdot f_{ir}$ (Soetaert et al., 1996a). However, here we do not consider this effect and set f_{ir} to a constant value of 1. The specific molecular diffusion coefficients $D_{\mathrm{mol},i}$ are corrected for sediment porosity ϕ, tortuosity F and are linearly interpolated for an ambient temperature T using zero-degree coefficients D_i^0 and temperature dependent diffusion coefficients D_i^T (compare Gypens et al., 2008):

$$D_{\mathrm{mol},i} = (D_i^0 + D_i^T \cdot T) \cdot \frac{1}{\phi \cdot F}$$

Tortuosity can be expresssed in terms of porosity as $F = \frac{1}{\phi^m}$ (Ullman and Aller, 1982) with the exponent m varying according to the type of sediment (here we use m=3). Values for D_i^T and D_i^0 are summarized in Table 9 and are adapted from Li and Gregory (1974) and Gypens et al. (2008).

2.4.2 Reaction Parameters and Stoichiometries

The applied multi-G approach for organic matter degradation considers specific degradation rate constants k_i (yr^{-1}) for each compound class which are assumed invariant along the sediment column and therefore independent of the nature of the terminal electron acceptor. The rate constants can be altered manually to fit observed sediment profiles (compare Section 3.1) or related to a master variable (e.g. sedimentation rate or POC-flux) provided by a coupled Earth System Model (compare Section 2.5.2 and 3.3). The rate constants for P related processes (i.e. sorption of $\mathrm{PO_4}$ to Fe oxides, release of $\mathrm{PO_4}$ from Fe-bound P due to Fe-oxide reduction and authigenic CFA precipitation) are k_s, k_m, k_a respectively. The pore water equilibrium concentrations for P sorption and CFA precipation ($\mathrm{PO_4}^s$, $\mathrm{PO_4}^a$) and the asymptotic concentration for Fe-bound P (M^∞) are taken from the Slomp et al. (1996). The stoichiometry of organic matter is represented by the factors $\mathrm{NC_i}$ and $\mathrm{PC_i}$ denoting the molecular nitrogen to carbon and phosphorus to carbon ratio. In the sulfidic and methanic zone the reduction of 1 mol organic matter additionally produces $\mathrm{SO_4C} = \frac{138}{212}$ mol of hydrogen sulfide and MC = 0.5 mol of methane. In the total sediment column organic matter mineralization consumes the specific TEA with a fixed ratio ($\mathrm{O_2C}$, $\mathrm{NO_3C}$ and $\mathrm{SO_4C}$ respectively). See Table 10 for a complete summary of the parameters and their values.

Table 9. Sediment characteristics and transport parameters. TODO: PO4 adsorption coefficients okay?

Parameter	Unit	Value	Description/Source
ρ_{sed}	$\mathrm{g\,cm^{-3}}$	2.6	Sediment density
w	$\mathrm{cm\,yr^{-1}}$	Fct. of seafloor	Advection/Sediment accumulation rate
		depth or from ESM	(Middelburg et al., 1997)
z_{bio}	cm	10 or 0.01	Bioturbation depth
			(Boudreau, 1998; Teal et al., 2010)
D_{bio}	$\mathrm{cm^2\,yr^{-1}}$	Fct. of seafloor	Bioturbation coefficient
		depth	(Middelburg et al., 1997)
ϕ	-	0.85	Porosity
F	-	$\frac{1}{\phi^m}$	Tortuosity, here m=3
f_{ir}	-	1	Irrigation factor
Adsorption coefficients			
$K_{\mathrm{NH_4}}$	-	1.3	NH_4 adsorption coefficient, (see Wang and Van Cappellen, 1996)
$K^{ox}_{\mathrm{PO_4}}$	-	200.0	PO_4 adsorption coefficient (oxic), (see Slomp et al., 1998)
$K^{anox}_{\mathrm{PO_4}}$	-	1.3	PO_4 adsorption coefficient (anoxic), (see Slomp et al., 1998)
Diffusion coefficients (Li and Gregory, 1974; Schulz, 2006; Gypens et al., 2008)			
$D^0_{\mathrm{O_2}}$	$\mathrm{cm^2\,yr^{-1}}$	348.62	Molecular diffusion coefficient of oxygen at 0°C
$D^T_{\mathrm{O_2}}$	$\mathrm{cm^2\,yr^{-1}\,{}^\circ C^{-1}}$	14.09	Diffusion coefficient for linear temp. dependence of oxygen
$D^0_{\mathrm{NO_3}}$	$\mathrm{cm^2\,yr^{-1}}$	308.42	Molecular diffusion coefficient of nitrate at 0°C
$D^T_{\mathrm{NO_3}}$	$\mathrm{cm^2\,yr^{-1}\,{}^\circ C^{-1}}$	12.26	Diffusion coefficient for linear temp. dependence of nitrate
$D^0_{\mathrm{NH_4}}$	$\mathrm{cm^2\,yr^{-1}}$	309.05	Molecular diffusion coefficient of ammonium at 0°C
$D^T_{\mathrm{NH_4}}$	$\mathrm{cm^2\,yr^{-1}\,{}^\circ C^{-1}}$	12.26	Diffusion coefficient for linear temp. dependence of ammonium
$D^0_{\mathrm{SO_4}}$	$\mathrm{cm^2\,yr^{-1}}$	157.68	Molecular diffusion coefficient of sulfate at 0°C
$D^T_{\mathrm{SO_4}}$	$\mathrm{cm^2\,yr^{-1}\,{}^\circ C^{-1}}$	7.88	Diffusion coefficient for linear temp. dependence of sulfate
$D^0_{\mathrm{H_2S}}$	$\mathrm{cm^2\,yr^{-1}}$	307.48	Molecular diffusion coefficient of sulfide at 0°C
$D^T_{\mathrm{H_2S}}$	$\mathrm{cm^2\,yr^{-1}\,{}^\circ C^{-1}}$	9.64	Diffusion coefficient for linear temp. dependence of sulfide
$D^0_{\mathrm{PO_4}}$	$\mathrm{cm^2\,yr^{-1}}$	112.91	Molecular diffusion coefficient of phosphate at 0°C
$D^T_{\mathrm{PO_4}}$	$\mathrm{cm^2\,yr^{-1}\,{}^\circ C^{-1}}$	5.59	Diffusion coefficient for linear temp. dependence of phosphate
D^0_{DIC}	$\mathrm{cm^2\,yr^{-1}}$	181.96	Molecular diffusion coefficient of DIC at 0°C
D^T_{DIC}	$\mathrm{cm^2\,yr^{-1}\,{}^\circ C^{-1}}$	8.66	Diffusion coefficient for linear temp. dependence of DIC
D^0_{ALK}	$\mathrm{cm^2\,yr^{-1}}$	181.96	Molecular diffusion coefficient of ALK at 0°C
D^T_{ALK}	$\mathrm{cm^2\,yr^{-1}\,{}^\circ C^{-1}}$	8.66	Diffusion coefficient for linear temp. dependence of ALK
Note: DIC and ALK coefficients are the mean values of HCO_3^-, CO_3^{2-} and CO_2 from Schulz (2006).			

Table 10. Values for biogeochemical parameters used in OMEN-SED. The variables x, y and z denote the atomic ratio of carbon, nitrogen and phosphorous of the degrading organic matter (here set to $C : N : P = 106 : 16 : 1$). P related coefficients okay?

Parameter/Variable	Unit	Value	Description
Stoichiometric factors and molecular ratios			
NC_i	mol/mol	$\frac{y}{x} = \frac{16}{106}$	nitrogen to carbon ratio
PC_i	mol/mol	$\frac{z}{x} = \frac{1}{106}$	phosphorus to carbon ratio
MC	mol/mol	0.5	methane to carbon ratio
			produced during methanogenesis
$DICC^{I}$	mol/mol	1.0	DIC to carbon ratio until z_{SO_4}
$DICC^{II}$	mol/mol	0.5	DIC to carbon ratio below z_{SO_4}
O_2C	mol/mol	$\frac{x+2y}{x} = \frac{138}{106}$	oxygen to carbon ratio
NO_3C	mol/mol	$\frac{4x+3y}{5x} = \frac{94.4}{106}$	nitrate to carbon ratio
SO_4C	mol/mol	$\frac{1}{2}O_2C = \frac{138}{212}$	sulfate to carbon ratio
ALK^{OX}	mol/mol	$\frac{y-2z}{x} = \frac{14}{106}$	ALK from aerobic degradation
ALK^{NIT}	mol/mol	-2	ALK from nitrification
ALK^{DEN}	mol/mol	$\frac{4x+3y-10z}{5x} = \frac{92.4}{106}$	ALK from denitrification
ALK^{SUL}	mol/mol	$\frac{x+y-2z}{x} = \frac{120}{106}$	ALK from sulfate reduction
ALK^{MET}	mol/mol	$\frac{y-2z}{x} = \frac{14}{106}$	ALK from methanogenesis
ALK^{H2S}	mol/mol	-2	ALK from H_2S oxidation
ALK^{AOM}	mol/mol	2	ALK from AOM
Secondary reaction parameters			
γ_{NH_4}	-	0.9	fraction of NH_4 that is oxidised
			in oxic layer
γ_{H_2S}	-	0.95	fraction of H_2S that is oxidised
			in oxic layer
γ_{CH_4}	-	0.99	fraction of CH_4 that is oxidised
			at z_{SO_4}
P related parameters			
k_s	yr^{-1}	1.0	Rate constant for PO_4 sorption
k_m	yr^{-1}	0.02	Rate constant for Fe-bound P release
k_a	yr^{-1}	10.0	Rate constant for authigenic CFA precipitation
${PO_4}^s$	$mol\,cm^{-3}$	$1 \cdot 10^{-9}$	equilibrium conc. for P sorption
			(Slomp et al., 1996)
${PO_4}^a$	$mol\,cm^{-3}$	$3.7 \cdot 10^{-9}$	equilibrium conc. for authigenic P precipitation
			(Slomp et al., 1996)
M^{∞}	$mol\,cm^{-3}$	$1.99 \cdot 10^{-10}$	asymptotic concentration for Fe-bound P
			(Slomp et al., 1996)

DH: ALK^{OX} correct?: y=NH4 prod.; -2z=P release

2.5 Module Structure

An analytical steady-state solution is found for the reaction-transport equation of each chemical species for every layer. At each boundary (i.e. $z_{\mathrm{ox}}, z_{\mathrm{bio}}, z_{\mathrm{NO_3}}$ and $z_{\mathrm{SO_4}}$) the model has to match continuity and flux for the ODE solutions of the layer above and below the specific boundary. In particular the bioturbation boundary is problematic as it can theoretically occur in any geochemical layer (compare Fig. 3). In order to simplify this recurring boundary matching problem it is implemented in an independent algorithm which is described in Section 2.5.1. Instructions and requirements for coupling OMEN-SED to a global Earth Sytem Model are given in Section 2.5.2.

2.5.1 Generic Boundary Condition Matching (GBCM)

A general steady-state advection-diffusion-reaction (ADR) diagenetic equation looks like:

$$\frac{\partial C}{\partial t} = 0 = D\frac{\partial^2 C}{\partial z^2} - w\frac{\partial C}{\partial z} - \sum_i \alpha_i \exp(-\beta_i z) - k \cdot C + Q. \tag{29}$$

where z is the sediment depth, t the time, D is the diffusion coefficient and w is the advection rate. The ODE solution is of the general form:

$$C(z) = A\exp(az) + B\exp(bz) + \sum_i \frac{\alpha_i}{D\beta_i^2 - w\beta_i - k} \cdot \exp(-\beta_i z) + \frac{Q}{k} \tag{30}$$

and can therefore be expressed as:

$$C(z) = A \cdot E(z) + B \cdot F(z) + G(z) \tag{31}$$

where $E(z)$, $F(z)$ are the homogeneous solutions of the ODE, G(z) the particular integral, and A, B are the integration constants (compare Fig. 3 for the whole sediment column).

Each boundary matching problem involves matching continuity and flux for the two solutions $C_U(z)$ (= 'upper') and $C_L(z)$ (= 'lower') across a boundary at $z = z_b$. Therefore, we get two ODE solutions of the genral form:

$$C_U(z) = A_U \cdot E_U(z) + B_U \cdot F_U(z) + G_U(z) \tag{32}$$

$$C_L(z) = A_L \cdot E_L(z) + B_L \cdot F_L(z) + G_L(z). \tag{33}$$

The two boundary conditions are: for continuity (where for generality we allow a discontinuity V_b)

$$C_U(z_b) = C_L(z_b) + V_b \tag{34}$$

and for flux

$$D_U C'_U(z_b) + wC_U(z_b) = D_L C'_L(z_b) + wC_L(z_b) + F_b \tag{35}$$

where w is advection, D are the diffusion coefficients and F_b is any flux discontinuity.

In terms of the ODE solutions (32), (33), the boundary conditions represent two equations connecting the four integration constants:

$$\begin{pmatrix} E_U & F_U \\ D_U E'_U & D_U F'_U \end{pmatrix} \begin{pmatrix} A_U \\ B_U \end{pmatrix} = \begin{pmatrix} E_L & F_L \\ D_L E'_L & D_L F'_L \end{pmatrix} \begin{pmatrix} A_L \\ B_L \end{pmatrix} + \begin{pmatrix} G_L - G_U + V_b \\ D_L G'_L - D_U G'_U + F_b - w V_b \end{pmatrix} \tag{36}$$

where the ODE solutions $E,\ F,\ G$ are all evaluated at z_b.

Equation (36) can be solved to give A_U and B_U as a function of the integration constants from the layer below (A_L and B_L), thereby constructing a piecewise solution for both layers, with just two integration constants.

In the code the function **benthic_utils.matchsoln** provides this solution in the form:

$$\begin{pmatrix} A_U \\ B_U \end{pmatrix} = \begin{pmatrix} c_1 & c_2 \\ c_3 & c_4 \end{pmatrix} \begin{pmatrix} A_L \\ B_L \end{pmatrix} + \begin{pmatrix} d_1 \\ d_2 \end{pmatrix}. \tag{37}$$

Using (37) we can now rewrite $C_U(z)$ in (32) as a function of A_L and B_L:

$$C_U(z) = (c_1 A_L + c_2 B_L + d_1) \cdot E_U(z) + (c_3 A_L + c_4 B_L + d_2) \cdot F_U(z) + G_U(z)$$

and hence define the "transformed" basis functions $E^*_U(z),\ F^*_U(z),\ G^*_U(z)$ such that:

$$C_U(z) = A_L \cdot E^*_U(z) + B_L \cdot F^*_U(z) + G^*_U(z) \tag{38}$$

where

$$\begin{aligned} E^*_U(z) &= c_1 E_U(z) + c_3 F_U(z) \\ F^*_U(z) &= c_2 E_U(z) + c_4 F_U(z) \\ G^*_U(z) &= G_U(z) + d_1 E_U(z) + d_2 F_U(z) \end{aligned} \tag{39}$$

(in the code this is done by **benthic_utils.xformsoln**).

Solving the sediment layer stack

Equations (37), (38) and (39) can now be applied for each layer boundary, working up from the bottom of the sediments. The net result is a piecewise solution of the whole sediment column with just two integration constants (coming from the lowest layer), which can then be solved for by applying one boundary condition for the sediment-water interface and one for the bottom of the sediments (e.g. a concentration condition at the SWI and a zero flux condition at z_∞).

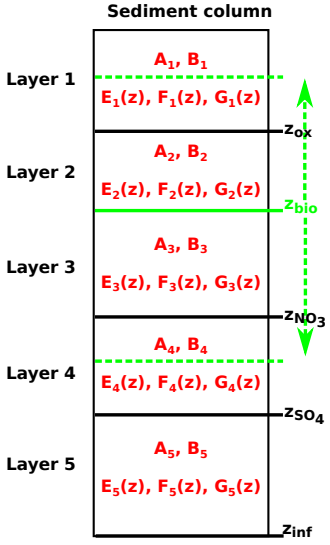

Figure 3. Schematic of the generic boundary condition matching (GBCM) problem. Showing the resulting integration constants ($A_i,\ B_i$) and ODE solutions ($E_i,\ F_i,\ G_i$) for the different sediment layers and the variable bioturbation boundary.

Abstracting out the bioturbation boundary

The bioturbation boundary affects the diffusion coefficient of the modelled solutes and the conservation equation of organic matter. The boundary is particularly inconvenient as it can, in principle, occur in the middle of any "geochemical" layer and therefore generates multiple cases (compare Fig. 3). To simplify this for solutes, the GBCM algorithm above is used to construct a piecewise solution and to abstract out the bioturbation boundary. An initial test for each "geochemical" layer is made to identify its "bioturbation-status" (fully bioturbated, fully non-bioturbated or crossing the bioturbation boundary) and (if needed) a piecewise solution is constructed by matching boundary conditions across the bioturbation boundary. The "outside" code therefore never needs to know whether it is dealing with a piecewise solution (i.e. matched across a bioturbation boundary) or a "simple" solution (i.e. the layer is fully bioturbated or fully non-bioturbated).

In the code, this is performed by **zTOC.prepfg_l12** which hands back a structure ls containing the "bioturbation-status" for each layer and (if needed) the description of the piecewise solution (coefficients $c_1, c_2, c_3, c_4, d_1, d_2$ as above). For example in the case of sulfate, **zTOC.prepfg_l12** is called three times before the actual profile is calculated (once per layer: oxic, suboxic, sulfidic) and hands back three structures ls with information about the layer's "bioturbation-status" and all associated conditional logic. When calculating the solutions for the different layers, the pre-calculated structure ls is passed to the function **zTOC.calcfg_l12** which sorts out the correct solution type to use.

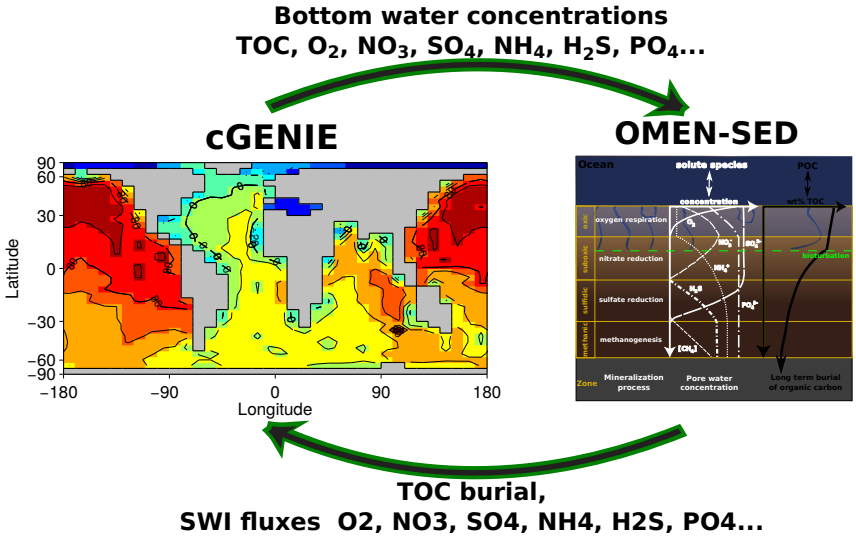

Figure 4. Schematic of the relationship between OMEN-SED and cGENIE. Arrows and accompanied text represent the information transferred between models.

2.5.2 Coupling to an Earth System Model

The coupling of OMEN-SED to the carbon-centric version of the "GENIE" Earth system model (cGENIE Ridgwell et al., 2007) is described (Fig. 4). Results from pre-industrial experiments are presented in Section 3.3. cGENIE is a model of Intermediate Complexity based on the efficient climate model "C-GOLDSTEIN" of Edwards and Marsh (2005), featuring a frictional-geostrophic 3D-ocean circulation model coupled to a fast Energy-Moisture Balance 2D-atmosphere together with a dynamic-thermodynamic sea-ice component. The version of cGENIE used here includes the marine geochemical cycling of carbon, oxygen, phosphorus and sulfur (Ridgwell et al., 2007), preservation of carbonates in deep-sea sediments (Ridgwell and Hargreaves, 2007) and terrestrial weathering (Colbourn et al., 2013). The ocean model is implemented on a 36×36 equal-area horizontal grid with 16 vertical levels using the pre-industrial continental configuration and bathymetry as in Archer et al. (2009). In contrast to Archer et al. (2009) the same grid resolution (36×36) is used for the sediment geochemistry model SEDGEM. Instead of completely remineralising POC at the seafloor, OMEN-SED is called by SEDGEM for each grid point. Depending on the overlying biogeochemical ocean model processes can be included or excluded in OMEN-SED and stoichiometric factors need to be adjusted to ensure preservation of mass. As nitrogen is not modelled explicitly in the employed cGENIE configuration the related stoichiometries in OMEN-SED are set to zero (i.e. $\mathrm{NC_i}$, $\mathrm{ALK^{NIT}}$ and $\mathrm{ALK^{DEN}}$). cGENIE, however, implicitly includes the effects of $\mathrm{NH_4}$ release and its nitrification on Alkalinity and neglects the impact of P release; therefore, related stoichiometries are changed to $\mathrm{ALK^{OX}} = -16/106$ and $\mathrm{ALK^{SUL}} = 122/106$.

Several biogeochemical tracers and parameters are transferred from SEDGEM to OMEN-SED and have to be converted into the required units. Bottom water concentrations of solutes are converted from $\mathrm{mol\,kg^{-1}}$ to $\mathrm{mol\,cm^{-3}}$ and the depositional flux of POC ($\mathrm{POC_{flux}}$) is converted from $\mathrm{cm^3\,cm^{-2}\,yr^{-1}}$ to $\mathrm{mol\,cm^{-2}\,yr^{-1}}$ assuming an average density of POC of $1.0\,\mathrm{cm^3\,g^{-1}}$. Other parameters used from cGENIE are seafloor depth, local temperature and the partitioning of bulk POC into the slower and faster degrading pool (as cGENIE represents a labile and a refractory POC fraction, see Ridgwell et al. (2007)). The advection/sediment accumulation rate is generally taken from cGENIE, however, a minimum values of $w = 0.5\,\mathrm{cm\,kyrs^{-1}}$ is imposed as OMEN-SED tends to be unstable for lower values. The bulk $\mathrm{POC_{flux}}$ is seperated into the labile and refractory component and the routine to calculate the sedimentary POC profiles is called. Here, the two POC depositional fluxes are first converted into SWI concentrations (in $\mathrm{mol\,cm^{-3}}$) by solving Eq. (3) for z=0. OMEN-SED computes the resulting SWI-fluxes of solutes (in $\mathrm{mol\,cm^{-2}\,yr^{-1}}$) and the fraction of POC preserved in the sediment at a depth of 100 cm ($\mathrm{POC_{pres}}$) and returns the results to cGENIE. In case no POC is deposited on the seafloor (i.e. $\mathrm{POC_{flux}} = 0$), OMEN-SED is not called and the SWI-fluxes of solutes and $\mathrm{POC_{pres}}$ are set to zero. In order to reduce memory requirements the sediment profiles (e.g. as shown in Fig. 5) are not calculated in the FORTRAN version of OMEN-SED, however, the boundary conditions are saved at the end of the experiment and sediment profiles for specific grid-cells, ocean basins and/or ocean transects can be plotted using the stand-alone matlab version of OMEN-SED.

3 Test Cases

TODO: Check Intro sentences To validate our approach, model results were compared with observed pore water profiles (Section 3.1), an extensive sensitivity analysis for the most important model parameters was performed and resulting sediment-water interface fluxes were compared with a global database (Section 3.2). Furthermore, OMEN-SED was coupled to the cGENIE Earth System model and different published parameterisations for the OM degradation rate constants are tested on a global scale (Section 3.3).

3.1 Sediment profiles

Modelled profiles were compared with measured pore water data from different ocean depths (Figure 5) including the continental shelf (108 m), upper slope (585 m), lower slope (2213 m) and the deep sea (4298 m). The site at 585 m depth located in the Santa Barbara Basin is characterised by anoxic bottom waters and high POC concentrations (POC $\sim$5.5 wt%, Reimers et al., 1996), whereas the other sites at the Iberian margin (108 and 2213 m) and the Nazaré Canyon (4298 m, Epping et al., 2002) are oxic. Sediment-water interface characteristics and concentrations of POC and dissolved species in OMEN-SED were set to the observed values where available (Table 11). The POC and

Table 11. Model boundary conditions for the sampling stations in Figure 5. (For all sites DIC bottom water concentration of 2,400 nanomole cm^{-3} is assumed.)

Sediment characteristics:							
Depth (m)	Temp. ($^{\circ}C$)	z_{bio} (cm)	D_{bio} ($cm^2 yr^{-1}$)	POC_1 (wt%)	POC_2 (wt%)	k_1 (yr^{-1})	k_2 (yr^{-1})
108	12.5	1.0	0.02	2.64	1.8	0.65	$1.0e^{-5}$
585	5.85	0.01	0.02	2.0	3.5	0.2	$8.0e^{-4}$
2213	3.2	10.0	0.17	0.45	0.5	0.1	$4.0e^{-4}$
4298	2.5	4.2	0.18	0.83	1.2	0.052	$1e^{-5}$

Bottom water concentrations of solutes (all in nanomole cm^{-3}):								
Depth	O_2	NO_3	SO_4	NH_4	H_2S	PO_4	PO_4^a	Alkalinity
108	210	9.6	28,000	0.4	0.0	0.0	15.0	2,400
585	10	25.0	28,000	0.0	0.0	50.0	90.0	2,480
2213	250	25.0	28,000	0.6	0.0	0.0	5.0	2,400
4298	243	30.1	28,000	0.22	0.0	0.0	5.0	2,400

pore water profiles were fitted by optimizing the POC partitioning into the fast and slow degrading pool and their respective first order degradation rate constants (priority given to reproduce the POC and O_2 profiles). For phosphorus the equilibrium concentration for authigenic P formation (PO_4^a) was adjusted to fit the PO_4 concentration at z_∞. For the two open Iberian margin stations (108 and 2213 m) OMEN-SED fits all observations well. OMEN-SED does especially well at depth 2213m by reproducing the deep O_2 penetration and the subsurface maximum in NO_3 concentration due to the nitrification of NH_4. For the Santa Barbara basin (585 m) a misfit is observed for H_2S and PO_4 in the upper 20 cm of the sediment. This can be explained by the presence of Mn^{2+}, Fe^{2+} and dissolved Fe at this site which are either reduced to degrade POC and/or react with H_2S to form iron sulfides, therefore inhibiting the rise in concentration of H_2S (Reimers et al., 1996). Phosphorus is adsorbed to Fe oxides and incorporated into carbonate fluorapatite (CFA) which is highly parameterised in OMEN-SED and not modelled explicitly. For the Nazaé Canyon station (4298 m) satisfactory fits could be realised apart from NH_4. However, also the original study (Epping et al., 2002) had the same problem using a more complex diagenetic model and suggested non-local solute exchange being responsible for the higher NH_4 concentrations at this site.

DH: P explanation correct/okay? Also, say something about [ALK] at 585m?

3.2 Sensitivity Analysis

Model parameters implicitly account for processes not explicitly described, they are notoriously difficult to constrain and a source of uncertainty for numerical and analytical models. One strategy to explore and quantify this model uncertainty that can always be applied is sensitivity analysis (SA). SA is a term used for mathematical techniques to investigate how the variations in the outputs

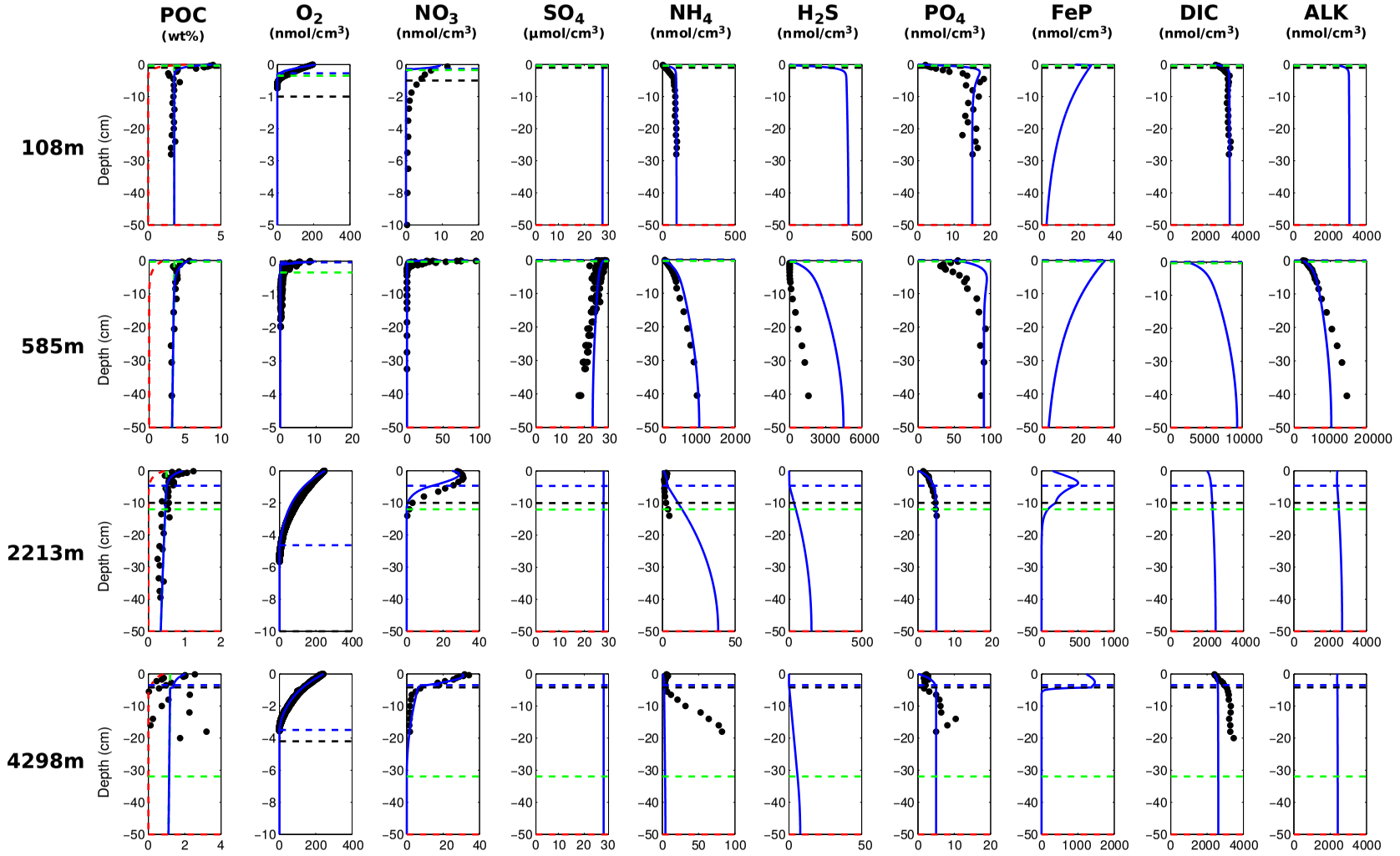

Figure 5. Modelled (curves) and measured (filled dots) dissolved and solid phase pore water profiles for four different sediment cores. Note that different scales are used for different stations. The blue POC curve represents the sum of the refractory (green) and labile (red) POC fraction.

(y_1, ..., y_N) of a model can be attributed to variations in the different input parameters (x_1, ..., x_M) (Pianosi et al., 2016). Different types of sensitivity indices, which quantify this relative influence with a scalar S_i, can be calculated, ranging from simple one-at-a-time methods to statistical evaluations of the output distribution (e.g. variance-based or density-based approaches Pianosi et al., 2016). Especially the latter indices are easy to interpret and can be compared across different parameters and/or different model outputs as they generally take values between zero and one ($S_i \in [0,1]$). An index of zero indicates a non-influential parameter and a higher value a more influential parameter. Here, we use SA mainly to identify which parameters have the largest impact on the different model outputs and therefore require careful calibration. As the probability density functions of our model outputs (i.e. the resulting SWI-fluxes) are generally highly-skewed towards extreme organic matter degradation rates (not shown) variance-based sensitivity indices are not very reliable uncertainty indicators (Pianosi et al., 2016). Rather than just considering the variance we employ the novel density-based PAWN method by (Pianosi and Wagener, 2015) which considers the entire conditional and unconditional Cumulative Destribution Function (CDF) of the model output. The sensitivity index of parameter i is calculated as the difference between the two CDFs, i.e.

$$S_i = \max_{x_i} \max_{y} |F_y(y) - F_{y|x_i}(y)| \tag{40}$$

where $F_y(y)$ is the unconditional CDF of the output y and $F_{y|x_i}(y)$ represents the conditional CDF when the i-th parameter is fixed to x_i. For a more detailed description of the method we refer the interested reader to Pianosi and Wagener (2015).

Due to the model complexity it is impossible to compute the sensitivity indices analytically therefore they are approximated from a Latin-Hypercube sampling of parameter inputs and calculated outputs. The PAWN method, as implemented within the Sensitivity Analysis for Everyone (SAFE) matlab toolbox (Pianosi et al., 2015), is used to investigate 11 model parameters for ranges as specified in Table 12. Sensitivity indices for all resulting SWI-fluxes for two idealised sediment conditions (i.e. anoxic at 400 m and oxic at 4000 m, see Table 13) are calculated. We use 200 samples to estimate the unconditional CDF, 100 samples to estimate the conditional CDFs and 10 conditioning points, thus 11,200 evaluations are performed for each sediment condition. The resulting indices (compare Fig. 9 in the Appendix) are then translated into a color code and summarised in a pattern plot to simplify comparison (Fig. 6). The most significant parameters for all model outputs are the degradation rate for the labile OM part ($\mathrm{k_1}$) and its share in the total OM pool ($\mathrm{f_1}$). For the anoxic setup, where no oxidation occurs, the secondary redox parameters (i.e. $\gamma_{\mathrm{NH_4}}$, $\gamma_{\mathrm{H_2S}}$) are essentially non-influential. Whereas in the oxic scenario, SWI-fluxes of $\mathrm{NH_4}$, $\mathrm{SO_4}$ and $\mathrm{H_2S}$ are very sensitive to changes in the secondary redox parameters. The $\mathrm{PO_4}$ SWI-flux appears to be insensitive especially under for the oxic condition as the majority is absorbed to Fe-oxides. The sensitivities change if other $\mathrm{PO_4}$ related equilibrium concentrations ${\mathrm{PO_4}}^s$, ${\mathrm{PO_4}}^a$ and M^∞ are used (not shown).

DH: explanation for small P sensitivity correct?

To test if OMEN-SED is able to reproduce the magnitude of observed SWI-fluxes, another set of Latin-Hypercube samplings is produced for the two idealised sediment conditions (sample sizes

Table 12. Range of model parameters used for sensitivity analysis of model predicted output.

Parameter	Description	Units	Minimum	Maximum	Source
$\mathrm{k_1}$	labile OM degradation constant	yr^{-1}	$1e^{-4}$	5.0	(1)
$\widetilde{\mathrm{k_2}}$	order of refractory OM degradation constant ($k_2 = \widetilde{k_2} \cdot k_1$)	-	$1e^{-4}$	$1e^{-1}$	(1)
$\mathrm{f_1}$	fraction of labile OM	-	0.02	0.98	-
$K_{\mathrm{NH_4}}$	Adsorption coefficient	-	0.8	1.7	(2)
$\gamma_{\mathrm{NH_4}}$	NH_4 fraction oxidised		0.5	1.0	-
$\gamma_{\mathrm{H_2S}}$	H_2S fraction oxidised		0.5	1.0	-
$K^{ox}_{\mathrm{PO_4}}$	Adsorption coeff. oxic	-	100.0	400.0	(3)
$K^{anox}_{\mathrm{PO_4}}$	Adsorption coeff. anoxic	-	1.3	2.0	(3)
k_s	kinetic P sorption	yr^{-1}	0.1	100.0	(4, 5)
k_m	Fe-bound P release	yr^{-1}	0.015	0.02	(4, 5)
k_a	authigenic P formation	yr^{-1}	0.001	10.0	(4, 6)

Sources: (1) Arndt et al. (2013); (2): Van Cappellen and Wang (1996); (3): Krom and Berner (1980) (4): Gypens et al. (2008); (5): Slomp et al. (1996); (6): Van Cappellen and Berner (1988)

Table 13. Model boundary conditions for the two idealised sediment conditions used for the sensitivity analysis (Fig. 6 and 7). All solute concentrations are in nanomole cm^{-3}.

Depth (m)	Temp. (°C)	OC (wt%)	O_2	NO_3	SO_4	PO_4	z_{bio} (cm)
400	8.0	2.0	0.0	40.0	28,000	40.0	0.001
4000	1.5	1.0	300.0	20.0	28,000	40.0	10.0

$N = 3500$) . Here the two most sensitive parameters $\mathrm{k_1}$ and $\mathrm{f_1}$ and also $\widetilde{\mathrm{k_2}}$ are varied, the other parameters are set to their default values (Tables 9 and 10). For the deep sea condition we account for the presence of more refractory OM by sampling $\mathrm{f_1} \in [0.02, 0.3]$. Minimum and Maximum values for the other parameters are as in Table 12. The results are compared with a global database of benthic fluxes of $\mathrm{O_2}$ and $\mathrm{NO_3}$ (Bohlen et al., 2012). The coloured scatter plots in Figure 7 show that the observed fluxes fall well in the range of SWI-fluxes calculated with OMEN-SED. Also highlighted by the emergence of colour patterns in Figure 7 A+B are the strong interactions between the amount of labile OM $\mathrm{f_1}$ and its degradation rate $\mathrm{k_1}$ for the resulting SWI-fluxes of the most powerful TEA available. In general, a higher degradation rate in combination with more labile OM available leads to a higher SWI-flux.

3.3 Pre-industrial cGENIE coupling and the OM degradation rate

OMEN-SED has been coupled to the global Earth system model cGENIE as described in Section 2.5.2. Our objective is not to perform and discuss a detailed calibration of the two models, as this

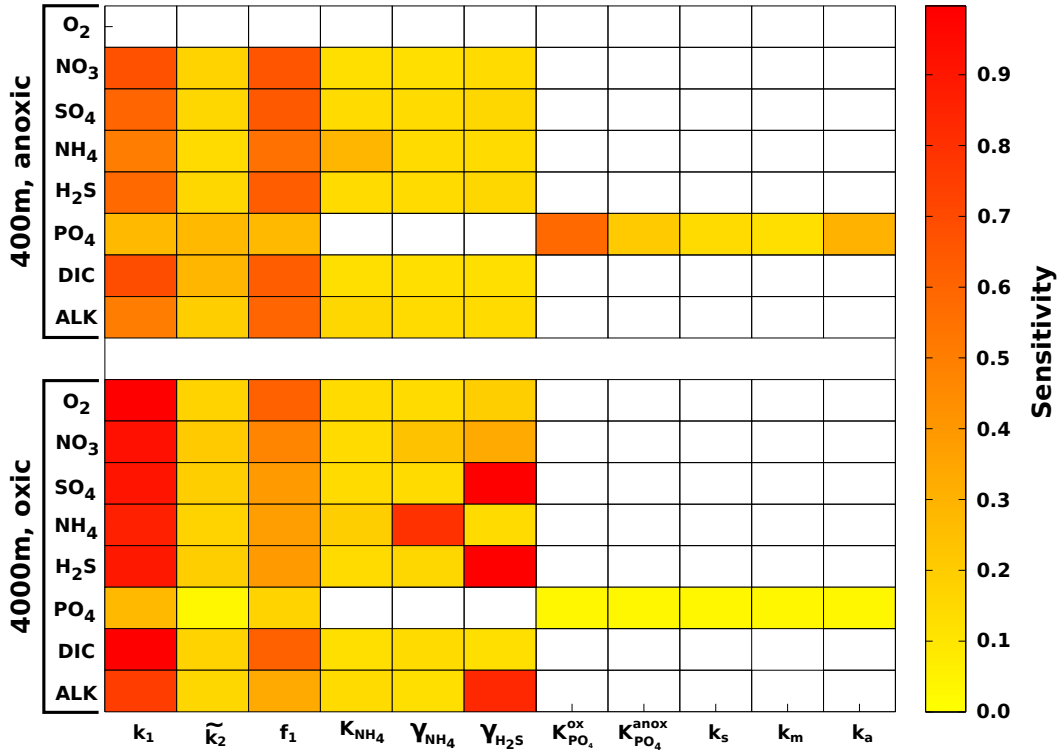

Figure 6. Pattern plot, showing the output sensitivity for each SWI flux (i.e. the chemical compounds on the horizontal axis) and each input factor (i.e. the model parameters on the vertical axis) for two idealised sediment cores. White patterns are assigned where the SWI flux is independent of the specific parameter.

DH: Rather low PO4 sensitivity - bc of Equil. concentr.?

is beyond the scope of this model development paper. We rather want to showcase, that a coupling is possible and results in general show main sediment features one would expect to see on a global scale. All simulations are run for 20,000 years to steady-state. OMEN-SED is called for each grid-cell in every time step, feeding back the resulting SWI-fluxes and the fraction of POC preserved in the sediments to cGENIE.

As discussed elsewhere (e.g. Arndt et al., 2013, and references therein) and also shown in our sensitivity analysis 3.2 of all the rate constants the degradation rates of OM (k_i) are the most influential parameters and strongly determine the SWI-flux of redox-sensitive elements. Thus, even though it is a major simplification, when coupling a diagenetic model to an ESM it is desirable to relate the OM degradation rates to a single, readily available characteristic (or master variable) of the local environmental conditions. For instance, considerable effort has been expended to relate the apparent rate constant for oxic and anoxic OM degradation to sedimentation rate (w) and various empirical relations have been proposed (Toth and Lerman, 1977; Tromp et al., 1995; Boudreau, 1997; Stolpovsky et al., 2015). We test globally invariant values as well as different published parameterisations for

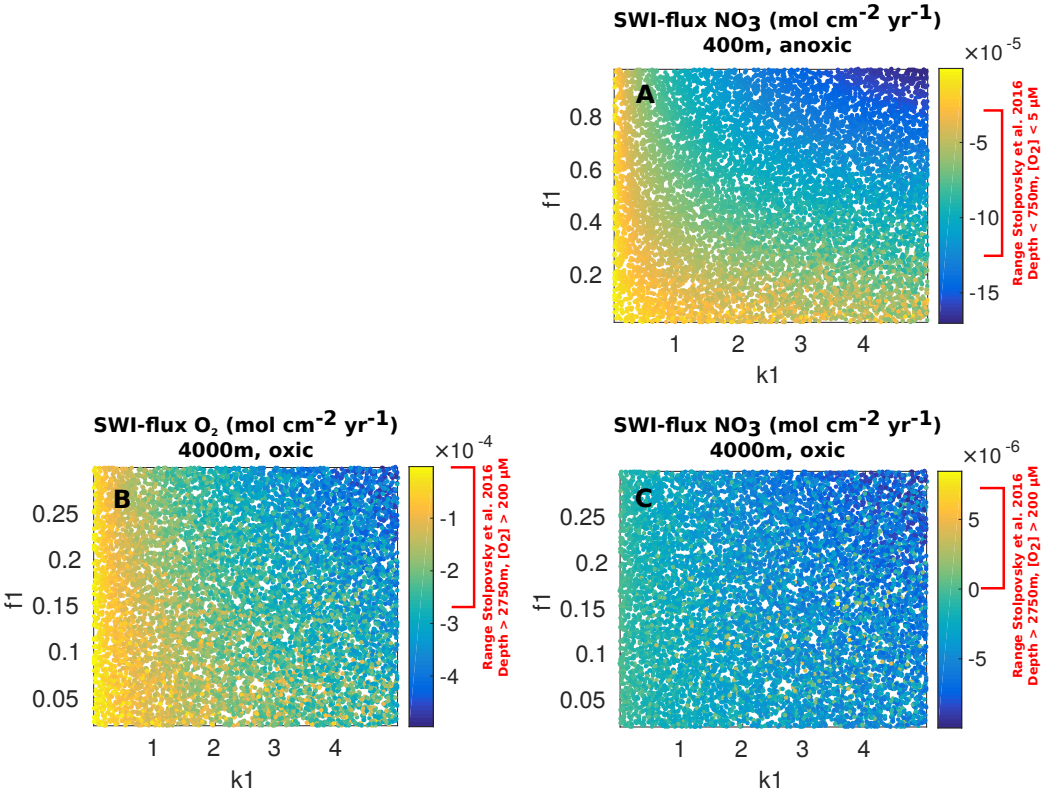

DH: Why mainly negative NO3-flux 4000m in contrast to database!?

Figure 7. Coloured scatter plots (k_1 vs f_1) of resulting OMEN-SED SWI-fluxes for the 400m anoxic (A: NO_3) and 4000m oxic (B: O_2, C: NO_3) scenario. Negative values representing a flux from the water column into the sediments. Indicated area in red at the respective colour scale represents the range of benthic fluxes in the global database of Bohlen et al. (2012).

the OM degradation rate constants (see Table 14) to test whether the different approaches are able to recreate main sediment characteristics. Depending on oxygen concentration in the bottom water, k_1 is defined as the oxic or anoxic degradation rate (anoxic for $[O_2] < 5$ nanomole cm^{-3}). The more refractory component is assumed to degrade one hundred times slower ($k_2 = k_1/100$, see e.g. Boudreau, 1997).

Describe Figure 8 and compare with what we know. E.g. Thullner et al. 2009!

Also check what water column features to show and maybe sediment P or Fe-P concentrations (see PALASTANGA et al. 2011, 2013).

Stolpovsky: bioturbated sediments deposited at continental margins quickly become anoxic within a few millimeters [Wenzhöfer and Glud, 2002].

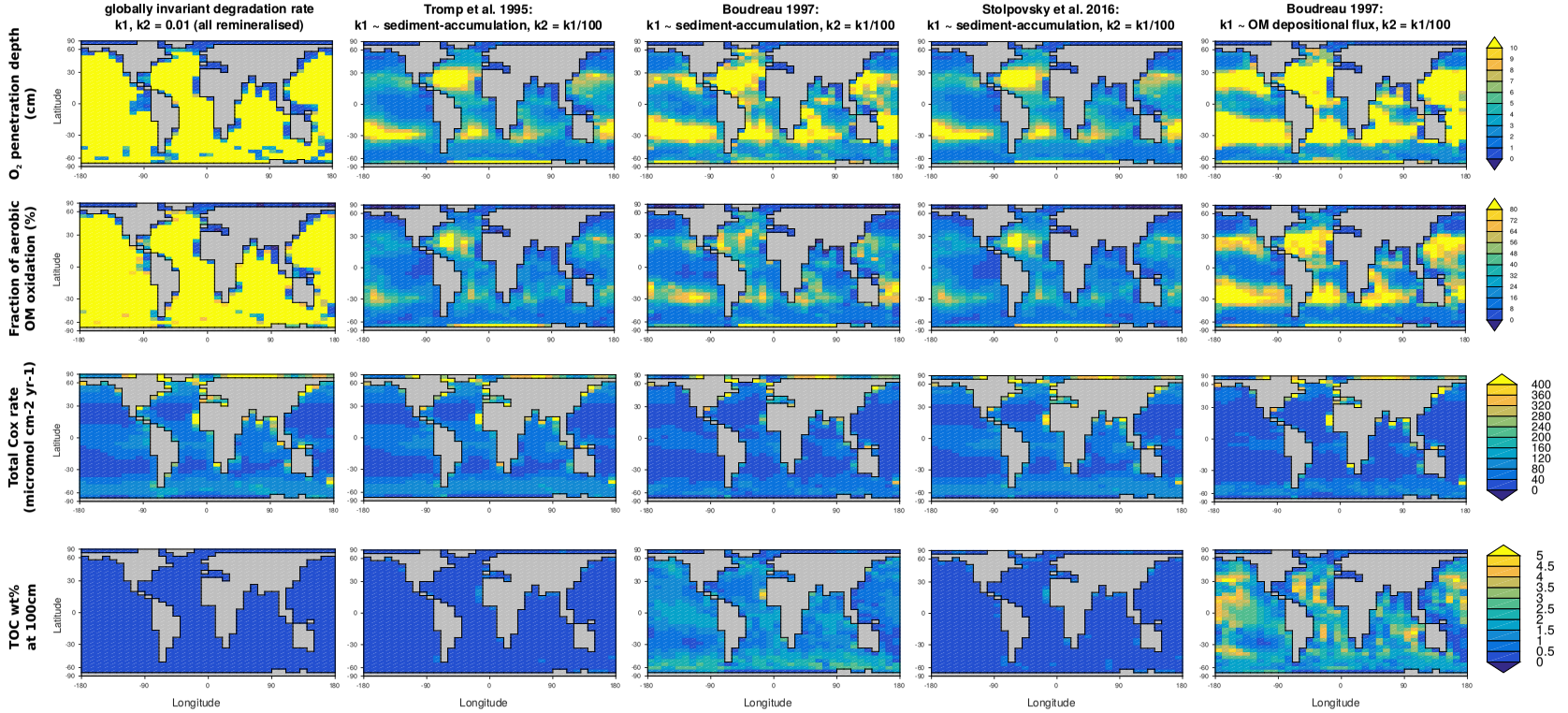

Figure 8. Results of OMEN-cGENIE coupling using different, published parameterisations for the OM degradation rates (k_1, k_2, compare Table **??**) coupled to the same cGENIE ocean setup. All results shown are sediment characteristics calculated by OMEN-SED. NOTE: Preliminary results (here frac2 still constant!) TODO: plot wt% just until 3%.

Table 14. List of coupled OMEN-cGENIE experiments with oxic and anoxic rate constants (k_1, yr^{-1}). The rate constant k_2 for the more refractory component is calculated as $k_2 = k_1/100$, apart from the Control experiment where $k_2 = 1.0$. D: seafloor depth.

Experiment	oxic rate constant	anoxic rate constant	Reference/Description
Control	1.0	1.0	All OM is remineralised.
Tromp	$2.97 \cdot w^{0.62}$	$0.057 \cdot w^{1.94}$	Tromp et al. (1995)
Boudreau_Toth	$0.38 \cdot w^{0.59}$	$0.04 \cdot w^2$	Boudreau (1997) oxic
			Toth and Lerman (1977) anoxic
Stolpovsky_Toth	$1.02 \cdot w^{0.5}$	$0.04 \cdot w^2$	Stolpovsky et al. (2015) oxic
			Toth and Lerman (1977) anoxic
Palastanga	0.01	0.008	$D \leq 2000$
	0.005	0.002	$D > 2000$ Palastanga et al. (2011)

4 Scope of applicability and model limitations

Stolpovsky:

- global parameterizations of biologically mediated transport and kinetic processes e.g. bioirrigation and nitrification rates. But no single set of biogeochemical and transport parameters is able to simulate all the shelf sites simultaneously

- globally invariant porosity, in reality permeability of sand is greater than fine-grained mud, such that boundary layer current and topography interactions will enhance the exchange of pore water with seawater by pressure-driven advective processes [Huettel et al., 1996]. N cycling in sands can thus exhibit large differences compared to fine-grained muds [e.g., Cook et al., 2006; Rao et al., 2007].

- Not able to simulate site specific seasonal variability in e.g. shallow sediments

- no globally realistic parameterisation for k

5 Conclusions

Not too bad this model...

Table 15. Primary pathways of organic matter degradation, secondary redox reactions and stoichiometries implemented in the reaction network.

Pathway	Stoichiometry
	Primary Redox reactions
Aerobic degradation	$(CH_2O)_x(NH_3)_y(H_3PO_4)_z + (x+2y)O_2 + (y+2z)HCO_3^- \rightarrow (x+y+2z)CO_2 + yNO_3^- + zHPO_4^{2-} + (x+2y+2z)H_2O$
Denitrification	$(CH_2O)_x(NH_3)_y(H_3PO_4)_z + \frac{(4x+3y)}{5}NO_3^- \rightarrow \frac{(2x+4y)}{5}N_2 + \frac{(x-3y+10z)}{5}CO_2 + \frac{(4x+3y-10z)}{5}HCO_3^- + zHPO_4^{2-} + \frac{(3x+6y+10z)}{5}H_2O$
Sulfate reduction	$(CH_2O)_x(NH_3)_y(H_3PO_4)_z + \frac{x}{2}SO_4^{2-} + (y-2z)CO_2 + (y-2z)H_2O \rightarrow \frac{x}{2}H_2S + (x+y-2z)HCO_3^- + yNH_4^+ + zHPO_4^{2-}$
Methanogenesis	$(CH_2O)_x(NH_3)_y(H_3PO_4)_z + (y-2z)H_2O \rightarrow \frac{x}{2}CH_4 + \frac{x-2y+4z}{2}CO_2 + (x-2z)HCO_3^- + yNH_4^+ + zHPO_4^{2-}$
	Secondary Redox reactions
Nitrification	$NH_4^+ + 2O_2 + 2HCO_3^- \rightarrow NO_3^- + 2CO_2 + 3H_2O$
Sulfide oxidation	$H_2S + 2O_2 + 2HCO_3^- \rightarrow SO_4^{2-} + 2CO_2 + 2H_2O$
AOM	$CH_4 + CO_2 + SO_4^{2-} \rightarrow 2HCO_3^- + H_2S$
	Adsorption reactions and mineral precipitation
NH_4 adsorption	$NH_4^+ \xrightarrow{K_{NH_4}} NH_4^+(ads)$
P ad-/desorption ???	$PO_4^{2-} \xrightarrow{K_{PO_4}^{I,II}} PO_4^{2-}(ads)$; $HPO_4^{2-} \xrightarrow{k_s} Fe-bound\ P \xrightarrow{k_m} HPO_4^{2-}$
CFA precipitation	$PO_4^{2-} \xrightarrow{k_a} CFA$

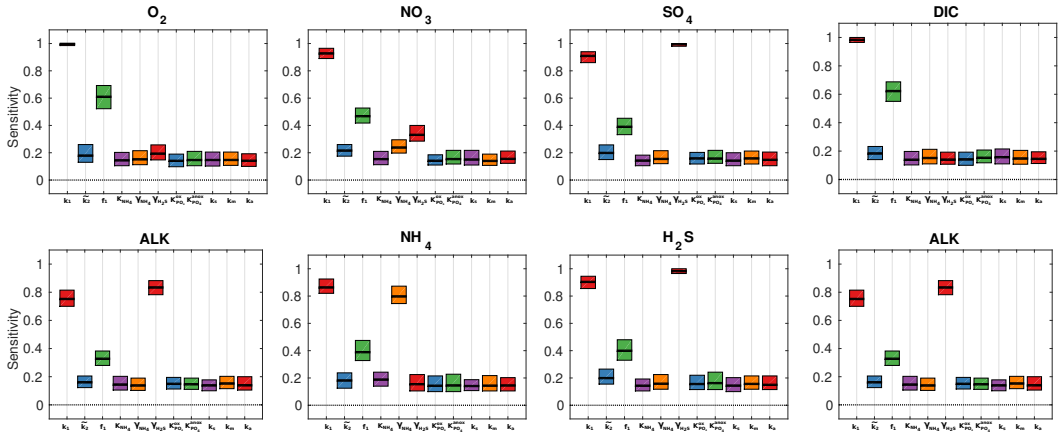

Figure 9. Move to Appendix Box plot of parameter sensitivities for the calculated SWI-fluxes for the 4000m oxic condition. Average sensitivities (black lines) and 90% confidence intervals using $N = 11200$ model evaluations and $Nboot = 100$ bootstrap resamples.

6 Code Availability

Appendix A: Reaction Network

Appendix B: Sensitivity Analysis

B1

Acknowledgements. Thank you...

References

Aguilera, D. R., Jourabchi, P., Spiteri, C., and Regnier, P. (2005). A knowledge-based reactive transport approach for the simulation of biogeochemical dynamics in Earth systems. *Geochemistry, Geophysics, Geosystems*, 6(7).

Archer, D., Eby, M., Brovkin, V., Ridgwell, A., Cao, L., Mikolajewicz, U., Caldeira, K., Matsumoto, K., Munhoven, G., Montenegro, A., and Tokos, K. (2009). Atmospheric Lifetime of Fossil Fuel Carbon Dioxide. *Annual Review of Earth and Planetary Sciences*, 37(1):117–134.

Archer, D. and Maier-Reimer, E. (1994). Effect of Deep-Sea Sedimentary Calcite Preservation on Atmospheric Co2 Concentration. *Nature*, 367(6460):260–263. 00506 WOS:A1994MR49400052.

Archer, D., Winguth, A., Lea, D., and Mahowald, N. (2000). What caused the glacial/interglacial atmospheric pCO2 cycles? *Reviews of Geophysics*, 38(2):159–189. 00414.

Arndt, S., Jørgensen, B., LaRowe, D., Middelburg, J., Pancost, R., and Regnier, P. (2013). Quantifying the degradation of organic matter in marine sediments: A review and synthesis. *Earth-Science Reviews*, 123:53–86.

Arthur, M. A., Dean, W. E., and Pratt, L. M. (1988). Geochemical and climatic effects of increased marine organic carbon burial at the Cenomanian/Turonian boundary. *Nature*, 335(6192):714–717.

Berner, R. A. (1964). An idealized model of dissolved sulfate distribution in recent sediments. *Geochimica et Cosmochimica Acta*, 28(9):1497–1503.

Berner, R. A. (1980). *Early Diagenesis: A Theoretical Approach*. Princeton University Press.

Berner, R. A. (2004). *The Phanerozoic Carbon Cycle: CO2 and O2*. Oxford University Press. 00000.

Billen, G. (1982). Modelling the processes of organic matter degradation and nutrients recycling in sedimentary systems. *Sediment microbiology*, pages 15–52.

Bohlen, L., Dale, A. W., and Wallmann, K. (2012). Simple transfer functions for calculating benthic fixed nitrogen losses and C:N:P regeneration ratios in global biogeochemical models. *Global Biogeochemical Cycles*, 26(3):GB3029.

Boudreau, B. P. (1996). A method-of-lines code for carbon and nutrient diagenesis in aquatic sediments. *Computers & Geosciences*, 22(5):479–496.

Boudreau, B. P. (1997). *Diagenetic models and their implementation*, volume 505. Springer Berlin.

Boudreau, B. P. (1998). Mean mixed depth of sediments: The wherefore and the why. *Limnology and Oceanography*, 43(3):524–526.

Boudreau, B. P. and Ruddick, B. R. (1991). On a reactive continuum representation of organic matter diagenesis. *American Journal of Science*, 291(5):507–538. 00187.

Burdige, D. J. (2006). *Geochemistry of marine sediments*, volume 398. Princeton University Press Princeton.

Colbourn, G., Ridgwell, A., and Lenton, T. M. (2013). The Rock Geochemical Model (RokGeM) v0.9. *Geosci. Model Dev.*, 6(5):1543–1573.

Edwards, N. R. and Marsh, R. (2005). Uncertainties due to transport-parameter sensitivity in an efficient 3-D ocean-climate model. *Climate Dynamics*, 24(4):415–433.

Emerson, S. and Bender, M. L. (1981). Carbon fluxes at the sediment-water interface of the deep-sea: calcium carbonate preservation. *Journal of Marine Research*, 39:139–162.

Epping, E., van der Zee, C., Soetaert, K., and Helder, W. (2002). On the oxidation and burial of organic carbon in sediments of the Iberian margin and Nazaré Canyon (NE Atlantic). *Progress in Oceanography*, 52(2–4):399–431.

Gehlen, M., Bopp, L., Emprin, N., Aumont, O., Heinze, C., and Ragueneau, O. (2006). Reconciling surface ocean productivity, export fluxes and sediment composition in a global biogeochemical ocean model. *Biogeosciences*, 3(4):521–537.

Goloway, F. and Bender, M. (1982). Diagenetic models of interstitial nitrate profiles in deep sea suboxic sediments. *Limnol. Oceanogr*, 27(4):624–638.

Goosse, H., Brovkin, V., Fichefet, T., Haarsma, R., Huybrechts, P., Jongma, J., Mouchet, A., Selten, F., Barriat, P.-Y., Campin, J.-M., Deleersnijder, E., Driesschaert, E., Goelzer, H., Janssens, I., Loutre, M.-F., Morales Maqueda, M. A., Opsteegh, T., Mathieu, P.-P., Munhoven, G., Pettersson, E. J., Renssen, H., Roche, D. M., Schaeffer, M., Tartinville, B., Timmermann, A., and Weber, S. L. (2010). Description of the earth system model of intermediate complexity LOVECLIM version 1.2. *Geosci. Model Dev.*, 3(2):603–633.

Gypens, N., Lancelot, C., and Soetaert, K. (2008). Simple parameterisations for describing n and p diagenetic processes: Application in the north sea. *Progress in Oceanography*, 76(1):89–110.

Heinze, C., Maier-Reimer, E., Winguth, A. M. E., and Archer, D. (1999). A global oceanic sediment model for long-term climate studies. *Global Biogeochemical Cycles*, 13(1):221–250.

Hensen, C., Zabel, M., and Schulz, H. N. (2006). Benthic Cycling of Oxygen, Nitrogen and Phosphorus. In Schulz, P. D. H. D. and Zabel, D. M., editors, *Marine Geochemistry*, pages 207–240. Springer Berlin Heidelberg.

Hülse, D., Arndt, S., Wilson, J., Munhoven, G., and Ridgwell, A. (2017). Understanding the causes and consequences of past marine carbon cycling variability through models. *Earth-Science Reviews*, –:in review.

Ilyina, T., Six, K. D., Segschneider, J., Maier-Reimer, E., Li, H., and Núñez-Riboni, I. (2013). Global ocean biogeochemistry model HAMOCC: Model architecture and performance as component of the MPI-Earth system model in different CMIP5 experimental realizations. *Journal of Advances in Modeling Earth Systems*, 5(2):287–315.

Ingall, E. and Jahnke, R. (1994). Evidence for enhanced phosphorus regeneration from marine sediments overlain by oxygen depleted waters. *Geochimica et Cosmochimica Acta*, 58(11):2571–2575. 00302.

Jahnke, R. A., Emerson, S. R., and Murray, J. W. (1982). A model of oxygen reduction, denitrification, and organic matter mineralization in marine sediments. *Limnol. Oceanogr*, 27(4):6–10.

Jarvis, I., Lignum, J. S., Gröcke, D. R., Jenkyns, H. C., and Pearce, M. A. (2011). Black shale deposition, atmospheric CO2 drawdown, and cooling during the Cenomanian-Turonian Oceanic Anoxic Event. *Paleoceanography*, 26(3):n/a–n/a.

Jenkyns, H. C. (2010). Geochemistry of oceanic anoxic events. *Geochemistry, Geophysics, Geosystems*, 11(3).

Krom, M. D. and Berner, R. A. (1980). Adsorption of phosphate in anoxic marine sediments1. *Limnology and Oceanography*, 25(5):797–806.

Lenton, T. M. and Watson, A. J. (2000). Redfield revisited: 1. Regulation of nitrate, phosphate, and oxygen in the ocean. *Global Biogeochemical Cycles*, 14(1):225–248.

Li, Y.-H. and Gregory, S. (1974). Diffusion of ions in sea water and in deep-sea sediments. *Geochimica et Cosmochimica Acta*, 38(5):703–714.

Mackenzie, F. T. (2005). *Sediments, Diagenesis, and Sedimentary Rocks: Treatise on Geochemistry, Second Edition*. Elsevier. 00000.

Meysman, F. J. R., Middelburg, J. J., Herman, P. M. J., and Heip, C. H. R. (2003). Reactive transport in surface sediments. II. Media: an object-oriented problem-solving environment for early diagenesis. *Computers & Geosciences*, 29(3):301–318. 00067.

Middelburg, J. J., Soetaert, K., and Herman, P. M. (1997). Empirical relationships for use in global diagenetic models. *Deep Sea Research Part I: Oceanographic Research Papers*, 44(2):327–344.

Mort, H. P., Adatte, T., Föllmi, K. B., Keller, G., Steinmann, P., Matera, V., Berner, Z., and Stüben, D. (2007). Phosphorus and the roles of productivity and nutrient recycling during oceanic anoxic event 2. *Geology*, 35(6):483–486. 00135.

Munhoven, G. (2007). Glacial–interglacial rain ratio changes: Implications for atmospheric and ocean–sediment interaction. *Deep Sea Research Part II: Topical Studies in Oceanography*, 54(5–7):722–746.

Najjar, R. G., Jin, X., Louanchi, F., Aumont, O., Caldeira, K., Doney, S. C., Dutay, J.-C., Follows, M., Gruber, N., Joos, F., Lindsay, K., Maier-Reimer, E., Matear, R. J., Matsumoto, K., Monfray, P., Mouchet, A., Orr, J. C., Plattner, G.-K., Sarmiento, J. L., Schlitzer, R., Slater, R. D., Weirig, M.-F., Yamanaka, Y., and Yool, A. (2007). Impact of circulation on export production, dissolved organic matter, and dissolved oxygen in the ocean: Results from Phase II of the Ocean Carbon-cycle Model Intercomparison Project (OCMIP-2). *Global Biogeochemical Cycles*, 21(3):GB3007.

Palastanga, V., Slomp, C. P., and Heinze, C. (2011). Long-term controls on ocean phosphorus and oxygen in a global biogeochemical model. *Global Biogeochemical Cycles*, 25(3):GB3024.

Pianosi, F., Beven, K., Freer, J., Hall, J. W., Rougier, J., Stephenson, D. B., and Wagener, T. (2016). Sensitivity analysis of environmental models: A systematic review with practical workflow. *Environmental Modelling & Software*, 79:214–232.

Pianosi, F., Sarrazin, F., and Wagener, T. (2015). A Matlab toolbox for Global Sensitivity Analysis. *Environmental Modelling & Software*, 70:80–85.

Pianosi, F. and Wagener, T. (2015). A simple and efficient method for global sensitivity analysis based on cumulative distribution functions. *Environmental Modelling & Software*, 67:1–11.

Reimers, C. E., Ruttenberg, K. C., Canfield, D. E., Christiansen, M. B., and Martin, J. B. (1996). Porewater pH and authigenic phases formed in the uppermost sediments of the Santa Barbara Basin. *Geochimica et Cosmochimica Acta*, 60(21):4037–4057.

Ridgwell, A. and Hargreaves, J. C. (2007). Regulation of atmospheric CO2 by deep-sea sediments in an Earth system model. *Global Biogeochemical Cycles*, 21(2):n/a–n/a.

Ridgwell, A., Hargreaves, J. C., Edwards, N. R., Annan, J. D., Lenton, T. M., Marsh, R., Yool, A., and Watson, A. (2007). Marine geochemical data assimilation in an efficient Earth System Model of global biogeochemical cycling. *Biogeosciences*, 4(1):87–104. 00090.

Schulz, H. D. (2006). Quantification of Early Diagenesis: Dissolved Constituents in Pore Water and Signals in the Solid Phase. In Schulz, P. D. H. D. and Zabel, D. M., editors, *Marine Geochemistry*, pages 73–124. Springer Berlin Heidelberg.

Shaffer, G., Malskær Olsen, S., and Pepke Pedersen, J. O. (2008). Presentation, calibration and validation of the low-order, DCESS Earth System Model (Version 1). *Geosci. Model Dev.*, 1(1):17–51. 00007.

Slomp, C., Malschaert, J., and Van Raaphorst, W. (1998). The role of adsorption in sediment-water exchange of phosphate in north sea continental margin sediments. *Limnology and Oceanography*, 43(5):832–846.

Slomp, C. P., Epping, E. H., Helder, W., and Van Raaphorst, W. (1996). A key role for iron-bound phosphorus in authigenic apatite formation in north atlantic continental platform sediments. *Journal of Marine Research*, 54(6):1179–1205.

Soetaert, K., Herman, P. M., and Middelburg, J. J. (1996a). Dynamic response of deep-sea sediments to seasonal variations: a model. *Limnology and Oceanography*, 41(8):1651–1668.

Soetaert, K., Herman, P. M. J., and Middelburg, J. J. (1996b). A model of early diagenetic processes from the shelf to abyssal depths. *Geochimica et Cosmochimica Acta*, 60(6):1019–1040.

Soetaert, K., Middelburg, J. J., Herman, P. M. J., and Buis, K. (2000). On the coupling of benthic and pelagic biogeochemical models. *Earth-Science Reviews*, 51(1–4):173–201.

Stein, R., Rullkötter, J., and Welte, D. H. (1986). Accumulation of organic-carbon-rich sediments in the Late Jurassic and Cretaceous Atlantic Ocean — A synthesis. *Chemical Geology*, 56(1–2):1–32.

Stolpovsky, K., Dale, A. W., and Wallmann, K. (2015). Toward a parameterization of global-scale organic carbon mineralization kinetics in surface marine sediments. *Global Biogeochemical Cycles*, 29(6):2015GB005087.

Teal, L., Bulling, M., Parker, E., and Solan, M. (2010). Global patterns of bioturbation intensity and mixed depth of marine soft sediments. *Aquatic Biology*, 2(3):207–218.

Toth, D. J. and Lerman, A. (1977). Organic matter reactivity and sedimentation rates in the ocean. *American Journal of Science*, 277(4):465–485.

Tromp, T. K., Van Cappellen, P., and Key, R. M. (1995). A global model for the early diagenesis of organic carbon and organic phosphorus in marine sediments. *Geochimica et Cosmochimica Acta*, 59(7):1259–1284. 00164.

Tsandev, I. and Slomp, C. (2009). Modeling phosphorus cycling and carbon burial during Cretaceous Oceanic Anoxic Events. *Earth and Planetary Science Letters*, 286(1–2):71–79.

Ullman, W. J. and Aller, R. C. (1982). Diffusion coefficients in nearshore marine sediments. *Limnology and Oceanography*, 27(3):552–556.

Van Cappellen, P. and Berner, R. A. (1988). A mathematical model for the early diagenesis of phosphorus and fluorine in marine sediments; apatite precipitation. *American Journal of Science*, 288(4):289–333.

Van Cappellen, P. and Ingall, E. D. (1994). Benthic phosphorus regeneration, net primary production, and ocean anoxia: A model of the coupled marine biogeochemical cycles of carbon and phosphorus. *Paleoceanography*, 9(5):677–692.

Van Cappellen, P. and Wang, Y. (1995). Metal cycling in surface sediments: modeling the interplay of transport and reaction. *Metal contaminated aquatic sediments*, pages 21–64.

Van Cappellen, P. and Wang, Y. (1996). Cycling of iron and manganese in surface sediments; a general theory for the coupled transport and reaction of carbon, oxygen, nitrogen, sulfur, iron, and manganese. *American Journal of Science*, 296(3):197–243.

Wang, Y. and Van Cappellen, P. (1996). A multicomponent reactive transport model of early diagenesis: Application to redox cycling in coastal marine sediments. *Geochimica et Cosmochimica Acta*, 60(16):2993–3014. 00283.

Wolf-Gladrow, D. A., Zeebe, R. E., Klaas, C., Körtzinger, A., and Dickson, A. G. (2007). Total alkalinity: The explicit conservative expression and its application to biogeochemical processes. *Marine Chemistry*, 106(1–2):287–300.